

1 Citation: **Hirt C**, Kuhn M, Featherstone WE, Göttl F (2012) Topographic/isostatic evaluation of new-generation
2 GOCE gravity field models, *J. Geophys. Res.*, 117, B05407, doi:10.1029/2011JB008878

3 4 **Topographic/isostatic evaluation of new-generation** 5 **GOCE gravity field models**

6
7 **C. Hirt**

8 Western Australian Centre for Geodesy & The Institute for Geoscience Research,
9 Curtin University of Technology, GPO Box U1987, Perth, WA 6845, Australia

10 Email: c.hirt@curtin.edu.au

11
12 **M. Kuhn**

13 Western Australian Centre for Geodesy & The Institute for Geoscience Research,
14 Curtin University of Technology, GPO Box U1987, Perth, WA 6845, Australia

15 Email: m.kuhn@curtin.edu.au

16
17 **W.E. Featherstone**

18 Western Australian Centre for Geodesy & The Institute for Geoscience Research,
19 Curtin University of Technology, GPO Box U1987, Perth, WA 6845, Australia

20 Email: w.featherstone@curtin.edu.au

21
22 **F. Göttl**

23 Deutsches Geodätisches Forschungsinstitut (DGFI),
24 Alfons-Goppel-Strasse 11, 80539 München, Germany

25 Email: goettl@dgfi.badw.de

26
27 **Abstract** We use gravity implied by the Earth's rock-equivalent topography (RET) and
28 modeled isostatic compensation masses to evaluate the new global gravity field models
29 (GGMs) from European Space Agency (ESA)'s Gravity Field and Steady-State Ocean
30 Circulation Explorer (GOCE) satellite gravimetry mission. The topography is now
31 reasonably well-known over most of the Earth's land masses, and also where conventional
32 GGM evaluation is prohibitive due to the lack (or unavailability) of ground-truth gravity data.
33 We construct a spherical harmonic representation of Earth's RET to derive band-limited
34 topography-implied gravity, and test the somewhat simplistic Airy/Heiskanen and
35 Pratt/Hayford hypotheses of isostatic compensation, but which did not improve the agreement
36 between gravity from the uncompensated RET and GOCE. The third-generation GOCE
37 GGMs (based on 12 months of space gravimetry) resolve the Earth's gravity field effectively
38 up to spherical harmonic degree ~200-220 (~90-100 km resolution). Such scales could not be
39 resolved from satellites before GOCE. From the three different GOCE processing
40 philosophies currently in use by ESA, the time-wise and direct approaches exhibit the highest
41 sensitivity to short-scale gravity recovery, being better than the space-wise approach. Our
42 topography-implied gravity comparisons bring evidence of improvements from GOCE to

43 gravity field knowledge over the Himalayas, Africa, the Andes, Papua New Guinea and
44 Antarctic regions. In attenuated form, GOCE captures topography-implied gravity signals up
45 to degree ~ 250 (~ 80 km resolution), suggesting that other signals (originating, e.g., from the
46 crust-mantle boundary and buried loads) are captured as well, which might now improve our
47 knowledge on the Earth's lithosphere structure at previously unresolved spatial scales.

48

49 **Keywords** GOCE, topography, gravity, rock-equivalent topography, isostasy

50

51 **1 Introduction**

52 The Gravity Field and Steady-State Ocean Circulation Explorer (GOCE) is the first
53 core mission of the “Living Planet” Earth observation programme by the European Space
54 Agency (ESA), e.g., *Drinkwater et al.* [2003]. The GOCE satellite was launched in March
55 2009 and entered its operational phase in September 2009. GOCE is the first mission to carry
56 a dedicated on-board three-axis gravity gradiometer at a low orbit altitude of ~ 260 km [*Bock*
57 *et al.*, 2011] attempting to resolve Earth's external gravity field with unprecedented detail
58 from space.

59 GOCE gravity field determination is based on the combination of satellite gravity
60 gradiometry (SGG) with satellite-to-satellite tracking (SST). SGG, used to measure the
61 second derivatives of the gravitational potential, is very sensitive to the medium-wavelength
62 components of the gravity field [e.g., *Rummel et al.*, 2011]. In solid-Earth geophysics,
63 GOCE SGG is expected to resolve regional mass-density anomalies that carry information on
64 the Earth's interior [e.g., *Marotta*, 2003; *Bagherbandi*, 2011; *Reguzzoni and Sampietro*
65 2012]. GPS-based SST provides high-accuracy information on the GOCE satellite orbit
66 geometry [*Bock et al.*, 2011] to complement the GOCE SGG in the long wavelengths.
67 GOCE's repeat cycle (the period to achieve full global data coverage) is ~ 2 months, and the
68 envisaged data collection period is expected to total ~ 40 months, from September 2009 til
69 December 2012 and possibly longer.

70 GOCE's mission target was to map gravity field features with 1-2 cm accuracy for
71 geoid undulations and ~ 1 mgal for gravity, down to scales of ~ 100 km, or spherical harmonic
72 degree ~ 200 . By comparison, geoid undulations from the EGM2008 global geopotential
73 model (GGM) [*Pavlis et al.*, 2008] are estimated to be accurate at the ~ 7 cm level (global
74 RMS). Over gravimetrically well-surveyed areas, the EGM2008 geoid accuracy can be at the
75 level of some cm [e.g., *Hirt et al.*, 2010a], while the accuracy degrades to the dm-level over
76 large parts of Asia, Africa, South America and Antarctica [*Pavlis et al.*, 2008]. In these
77 EGM2008 ‘problem areas’, *Pavlis et al.* [2008] did not have high-resolution terrestrial
78 gravity data (12% of land) or only had access to proprietary data (43% of land). It is these
79 regions devoid of dense sets of terrestrial gravity observations where GOCE is expected to
80 add most significantly to terrestrial gravity field knowledge.

81 ESA has made available GOCE GGMs based on ~ 2 months (herein first-generation),
82 ~ 8 months (second-generation) and ~ 12 months (third-generation) of observation data, based
83 on three different strategies for gravity field recovery [e.g., *Pail et al.*, 2011], see Section 2.
84 The performance of the first-generation GGMs has been evaluated by different strategies.
85 *Gruber et al.* [2011] investigated GOCE-implied orbit residuals of various geodetic satellites

86 and compared GOCE GGMs against ground-truth geoid undulations. *Hirt et al.* [2011]
87 utilized regional land gravity and vertical deflections as ground-truth to assess GOCE gravity
88 field information. Differences between GOCE GGMs and EGM2008 (from the pre-GOCE-
89 era) were analysed by *Hirt et al.* [2011] and *Pail et al.* [2011], and inferences were made but
90 no direct evidence obtained for GOCE-conferred improvements over the EGM2008 ‘problem
91 areas’.

92 The aim of this study is to use gravity implied by the Earth’s topography and models
93 of its isostatic compensation masses to assess the new-generation GOCE model performance
94 over the Himalayas, Africa, Andes, Papua New Guinea and Antarctica. We exploit the
95 relatively good knowledge of topography over most of the Earth’s surface (through digital
96 elevation models) along with GOCE’s sensitivity to the gravitational attraction of
97 topographic masses [*Wild and Heck, 2005; Makhloof and Ilk 2008; Janák et al., 2012*] to
98 bring - for the first time - direct evidence for GOCE gravity field improvements in regions
99 where terrestrial gravity data are restricted.

100 Based on topographic heights over land areas, ocean depths, ice shield thickness data,
101 we construct rock-equivalent topography (RET; *Rummel et al.* [1988]) and derive RET-
102 implied gravity to approximate the gravitational attraction of Earth’s topography and some of
103 Earth’s major mass-density anomalies. Some focus is placed on ways to account for isostatic
104 compensation of the topography [e.g., *Watts, 2001*]. The gravitational effect from the
105 isostatic compensation masses is approximated and tested here based on the Crust 2.0
106 lithosphere model [*Bassin et al., 2000*], the classical Airy/Heiskanen and Pratt/Hayford
107 hypotheses and a combination of them (Section 3). The relationship between GOCE-
108 measured and topography/isostasy-implied gravity is not only analyzed using correlation
109 coefficients, but also based on a new criterion termed reduction rates. These quantify the
110 extent of topography-implied gravity signals captured by the GOCE GGMs at different
111 spatial scales (i.e., as a function of harmonic degree). Reduction rates are introduced and
112 used because they are more sensitive than correlation coefficients to identify topography-
113 generated signals in the GGMs (Section 4).

114 Gravity implied by RET not only allows for identification of GOCE-conferred gravity
115 field improvements over EGM2008 ‘problem areas’, but also global and regional evaluation
116 of the GOCE gravity recovery strategies. Using RET as a single, globally homogeneous
117 reference data set, our analyses provide independent feedback on the ability of the ESA
118 GOCE gravity processing strategies to recover short-scale gravity signals. While *Pail et al.*
119 [2011] state that “*due to the fact that the [three] models are based on different processing*
120 *philosophies [...] they cannot and should not be compared directly*”, we believe that users are
121 interested to know how the different GOCE models perform both in an absolute and relative
122 sense. Comparisons between uncompensated and compensated RET demonstrate that the
123 classical hypotheses of isostatic compensation are of limited use to model isostasy globally at
124 the spatial scales resolved by GOCE. Comparisons with uncompensated RET-implied
125 gravity show the performance differences of the three GOCE gravity recovery strategies, and
126 demonstrate the sensitivity of GOCE gradiometry for short-scale gravity recovery at spatial
127 scales down to ~80 km, which also has future applications in solid Earth geophysics, e.g., the
128 improvement of lithosphere models at short scales (Sections 4, 5).

129
 130
 131
 132
 133
 134

2 Data sets

2.1 GOCE Gravity Field Models

Table 1. Global gravity field models tested

Model name	Degree	GOCE Data	Other data ¹	Reference
GOCE-DIR3 ^a	240	~12 months	LAGEOS and GRACE to degree 160 from GRGS RL02 (Bruinsma et al. 2009)	Bruinsma et al. (2010)
GOCE-DIR2 ^b	240	8 months	ITG-Grace2010s to degree 150	Bruinsma et al. (2010)
GOCE-DIR1 ^c	240	2 months	EIGEN51C (GRACE, CHAMP, G,A) at all scales	Bruinsma et al. (2010)
GOCE-SPW2 ^d	240	8 months	N/A	Migliaccio et al. (2010)
GOCE-SPW1 ^e	210	2 months	EGM2008 (GRACE, G,A) at low degrees	Migliaccio et al. (2010)
GOCE-TIM3 ^f	250	~12 months	N/A	Pail et al. (2011)
GOCE-TIM2 ^g	250	8 months	N/A	Pail et al. (2011)
GOCE-TIM1 ^h	224	2 months	N/A	Pail et al. (2010)
ITG-Grace2010s	180	-	7 years GRACE	Mayer-Gürr et al. (2010)

135
 136
 137
 138
 139
 140
 141
 142
 143
 144
 145
 146
 147
 148
 149
 150
 151
 152
 153
 154
 155
 156

- a ESA name GO_CONS_EGM_GCF_2__20091101T000000_20110419T235959_0001
- ICGEM name GOC_CONS_GCF_2_DIR_R3
- b ESA name GO_CONS_EGM_DIR_2I_20091101T000000_20100630T235959_0001
- ICGEM name GOC_CONS_GCF_2_DIR_R2
- c ESA name EGM_GOC_2__20091101T000000_20100110T235959_0002
- ICGEM name GOC_CONS_GCF_2_DIR_R1
- d ESA name GO_CONS_EGM_SPW_2I_20091031T000000_20100705T235959_0001
- ICGEM name GOC_CONS_GCF_2_SPW_R2
- e ESA name EGM_GOC_2__20091030T005757_20100111T073815_0002
- ICGEM name GOC_CONS_GCF_2_SPW_R1
- f ESA name GO_CONS_EGM_GCF_2__20091101T000000_20110430T235959_0001
- ICGEM name GOC_CONS_GCF_2_TIM_R3
- g ESA name GO_CONS_EGM_TIM_2I_20091101T000000_20100705T235500_0001
- ICGEM name GOC_CONS_GCF_2_TIM_R2
- h ESA name EGM_GOC_2__20091101T000000_20100111T000000_0002
- ICGEM name GOC_CONS_GCF_2_TIM_R1
- i Abbreviations: G = terrestrial gravity, A = gravity from altimetry.

157 The spherical harmonic coefficients of eight GOCE-based GGMs from the GOCE
 158 High-Level Processing Facility (HPF) have been released publically via ESA
 159 (<http://www.esa.int>) and the International Centre for Global Earth Models (ICGEM,
 160 <http://icgem.gfz-potsdam.de/ICGEM/>). Table 1 gives an overview of their formal resolution
 161 (i.e., the maximum spherical harmonic degree published), the data used to derive the model

162 coefficients, and the corresponding citations. As a benchmark of the pre-GOCE-era, one
163 GRACE (Gravity and Climate Change Experiment; *Tapley et al.* [2004])-based model (ITG-
164 GRACE2010s, using seven years of GRACE observations, cf. *Mayer-Gürr et al.* [2010]) is
165 also included.

166 The eight GOCE GGMs are based on three different processing philosophies [*Pail et al.*,
167 2011]: the direct approach (DIR), space-wise approach (SPW) and time-wise approach
168 (TIM). Each approach has been applied to ~2 months (first-generation), ~8 months (second-
169 generation) and ~12 months (third-generation) of GOCE gradiometry and GPS-derived
170 orbits. Below are the basic concepts and most important differences among the approaches,
171 inferred from *Pail et al.* [2011] and the header information in the coefficient files from
172 ICGEM.

- 173 • The DIR and TIM approaches use the least-squares solution of the inverse problem,
174 where GOCE observations (gradiometry and GPS orbits) are related to the unknown
175 parameters (spherical harmonic coefficients of Earth’s gravity field) via large systems of
176 normal equations. Their direct inversion generally requires the use of supercomputers.
- 177 • The DIR-approach makes use of an *a priori* GGM (cf. Table 1) and adds GOCE
178 observations to improve it. An important difference between first- and second/third-
179 generation DIR models, GOCE-DIR1 incorporates *a priori* information from the
180 combined EIGEN-51C model [*Bruinsma et al.*, 2010] at all spatial scales. As such,
181 GOCE-DIR1 relies on other satellite data at long scales and terrestrial gravity at short
182 scales. Opposed to this, GOCE-DIR2 uses the GRACE-only-derived model ITG-
183 GRACE2010s (cf. Table 1) as an *a priori* GGM to degree 150, so is a pure GOCE-only
184 GGM beyond this degree. GOCE-DIR3 uses LAGEOS Satellite Laser Ranging and the
185 GRGS GRACE model [*Bruinsma et al.*, 2009] gravity field as an *a priori* to degree 160.
- 186 • No *a priori* gravity field information is used in the GGMs derived from the TIM
187 approach, but Kaula regularisation (an empirical law on the decay of the Earth’s gravity
188 spectrum with altitude, cf. *Kaula* [1966]) is applied to constrain the TIM1, TIM2 and
189 TIM3 GGM coefficients at short scales. The TIM processing philosophy delivers pure
190 GOCE-only models that are independent of *a priori* gravity field data.
- 191 • In the SPW approach, GOCE observations are gridded at satellite altitude by means of
192 least-squares collocation. The spherical harmonic coefficients are obtained through a
193 spherical harmonic analysis of the gridded observations. EGM2008 is incorporated into
194 GOCE-SPW1 as an *a priori* model only at very long wavelengths, so it can be
195 considered as a pure GOCE-only model at medium and shorter scales. According to the
196 ICGEM file information, GOCE-SPW2 does not use *a priori* gravity field information.
197 GOCE-SPW3 is not yet publicly available.

198 In summary, GOCE-TIM1,2&3 and GOCE-SPW2 are pure GOCE-only models at all
199 spatial scales, and GOCE-SPW1 is GOCE-only apart from the very long wavelengths.
200 GOCE-DIR2,3 are GOCE-only models at short scales and GOCE-DIR1 is a mixed product
201 that is underpinned by various prior gravity field sources.

202 We acknowledge that ‘combined satellite-only’ GGMs (e.g., GOCO01S, *Pail et al.*
203 [2010], GOCO02S, *Goiginger et al.* [2011] and EIGEN-6, *Förste et al.* [2011]) have been
204 developed based on GOCE and GRACE. Such GGMs are superior to GOCE-only models

205 due to incorporating highly-accurate GRACE models at long wavelengths (and/or other
206 satellite data), cf. *Pail et al.* [2010]. Given that the GOCE component of these combined
207 satellite-only GGMs is similar or identical to the ESA GOCE products, we limit our study to
208 the GGMs in Table 1.

209

210 **2.2 Topography**

211 We use the spherical harmonic expansion of the DTM2006.0 digital elevation data
212 [*Pavlis et al.*, 2007], a co-product of EGM2008 [*Pavlis et al.*, 2008]. It contains (i) the
213 Shuttle Radar Topography Mission (SRTM, *Farr et al.*, [2007]) data over land within
214 latitudes of 56° South and 60° North, (ii) ICESat-2 laser altimetry [*Abdalati et al.*, 2010] over
215 Greenland and Antarctica, (iii) bathymetry derived from altimetry and ship depth soundings
216 [*Smith and Sandwell*, 1997], and (iv) DTM2002 elevation data [*Saleh and Pavlis*, 2003]
217 elsewhere. Spherical harmonic coefficients of the topography, derived to degree 2700 from
218 2'×2' DTM2006.0 mean values, are publicly available to degree 2160 via [http://earth-](http://earth-info.nga.mil/GandG/wgs84/gravitymod/egm2008/)
219 [info.nga.mil/GandG/wgs84/gravitymod/egm2008/](http://earth-info.nga.mil/GandG/wgs84/gravitymod/egm2008/).

220 In order to better RET-model the ice sheets over Greenland and Antarctica, we use the
221 bedrock information contained in the global 1'×1' ETOPO1 relief model [*Amante and Eakins*,
222 2009]. Over Greenland, bedrock elevations are obtained indirectly through ice surface and
223 ice thickness information provided by the National Snow and Ice Data Centre (NSIDC)
224 [*Bamber et al.*, 2001]. The ice surface is the result of the combination of radar altimetry and
225 airborne data, where the ice thickness is obtained from airborne ice-penetrating radar. Over
226 Antarctica, BEDMAP describes the bedrock elevation under the grounded ice sheets [*Lythe et*
227 *al.*, 2000]. This is based primarily on the gridding of radar and seismic soundings.

228

229 **3 Methodology**

230 **3.1 Introductory Remarks**

231 The basic idea of this study is to compare gravity signals, as measured by GOCE and
232 implied by Earth's topography and models of its isostatic compensating masses, at various
233 spatial scales. For this purpose, we construct a spherical harmonic representation of Earth's
234 topography, cryosphere and hydrosphere based on a uniform mass-density (Section 3.2),
235 derive its gravitational potential (Section 3.3) and gravity disturbances (Section 3.4) that are
236 compared over a range of spectral bands (Section 4), allowing us analyses of GOCE's
237 sensitivity for topography-generated gravity signals, specifically at short spatial scales that
238 have never been measured from space before.

239 GOCE is not only sensitive to the gravitational attraction of the Earth's visible
240 topography, but also to its isostatic compensation masses [e.g., *Wild and Heck*, 2005;
241 *Makhlof and Ilk*, 2008]. This raises the question of how to account for isostatic
242 compensation in the comparisons between GOCE and Earth's topography. An initial strategy
243 is to consider the topography as isostatically uncompensated or supported by the rigidity of
244 the lithosphere, which, according to *Wieczorek* [2007], should be a “good approximation”
245 above harmonic degree ~200. To model isostatic compensation of the topographic masses,
246 commonly used strategies are available that are based on

247

- 248
- 249
- 250
- 251
- 252
- 253
- 254
- 255
- 256
- 257
- 258
- 259
- 260
- 261
- 262
- 263
- 264
- 265
- 266
- 267
- 268
- Simplistic compensation models, such as those of Airy-Heiskanen (A/H) or Pratt-Hayford (P/H) [e.g., *Heiskanen and Moritz*, 1967; *Torge*, 2001; *Göttl and Rummel* 2009]. The A/H and P/H models (Section 3.3) assume local compensation of the topography loads and an intrinsically weak crust [e.g., *Watts*, 2001], so are sometimes crude simplifications of the actual lithospheric properties. It is important to note that both the A/H and P/H compensation models offer [formally] a spatial resolution comparable to that of the topography model, so possess short-scale spectral energy which is a prerequisite for comparisons with GOCE.
 - More regional compensation models of Vening-Meinesz also take into account the flexural rigidity of the lithosphere [e.g., *Watts*, 2011]. Regional compensation models imply that loads larger than a certain transition wavelength are compensated while smaller topographic features are supported mechanically by the lithosphere. The transition wavelength depends upon, among other parameters, the elastic thickness T_e .
 - Crustal thicknesses estimates, e.g., from seismic refraction data such as the Crust 2.0 lithosphere model [*Bassin et al.*, 2000], or effective elastic thickness estimates from admittance and coherence studies [e.g., *Watts*, 2001, p 416f]. However, neither the Crust 2.0 resolution ($2^\circ \times 2^\circ$ corresponding to spherical harmonic degree of 90), nor the resolution or accuracy of global elastic thickness maps [see *Watts*, 2001, p 418] are of sufficient resolution to provide feedback on GOCE observations at ~ 100 km spatial scales (equivalent to harmonic degree of 200).

269

270

271

272

273

274

275

276

277

278

To our knowledge, there is currently no global crustal thickness model available of sufficient resolution that would allow us to account for and model isostatic compensation effects at or near the GOCE spatial resolution of ~ 100 km, without having to rely on simplified hypotheses such as those behind the A/H or P/H models. Vening-Meinesz-type models rely on the core assumption that local topographic loads are supported mechanically by the lithosphere, so are very similar to the uncompensated topography (option 1 below) at short spatial scales, and are not included here. The limited resolution of crustal thickness models (option 5 below) is exemplified in Sect. 4.2. In the absence of “observation-based” crustal thickness models of sufficiently high spatial resolution, we are restricted to test the following five modelling variants of Earth’s topography and its isostatic compensation:

- 279
- 280
- 281
- 282
- 283
- 284
- (1) uncompensated [rock-equivalent] topography, ice and oceans,
 - (2) A/H isostatic compensation plus the effect of (1),
 - (3) P/H isostatic compensation plus the effect of (1),
 - (4) A combination of A/H and P/H, that uses A/H over the continents and P/H over the oceans, plus the effect of (1),
 - (5) the Crust 2.0 lithosphere model.

285

286

Also because of the lack of a high-resolution 3D density model of the crust and lithosphere, we are unable to account for the isostatic compensation of mass anomalies.

287 **3.2 Rock-equivalent topography**

288

289

290

RET is a representation of Earth’s topography that “compresses” ocean water and ice into layers equivalent to the mass-density of topographic rock (using the frequently presumed mean value of 2670 kg m^{-3}), while keeping the water and ice masses constant. RET allows

291 computation of implied gravity effects based on a single constant uniform mass-density over
 292 land, ocean areas and ice shields.

293 For our topography-based GOCE GGM evaluation, RET is required in a spherical
 294 harmonic representation. The published version of DTM2006.0 [Pavlis *et al.*, 2007;
 295 http://earth-info.nga.mil/GandG/wgs84/gravitymod/egm2008/first_release.html] cannot be
 296 used directly because it describes the surface of the solid Earth above or below local mean
 297 sea level. Over Greenland and Antarctica, DTM2006.0 heights are reckoned to the top of the
 298 ice shields so the incorrect RET would be assigned to ice masses; likewise for the oceans. As
 299 such, the scheme depicted in Fig. 1 is used to appropriately assign mass densities to ice and
 300 ocean water. We have constructed a RET in the spatial domain that accounts for the effect of
 301 the ocean water masses and ice shields over Greenland and Antarctica, and derived its
 302 spherical harmonic coefficients. The construction, which we name RET2011, was based on
 303 following three-step procedure.

304 First, a $5' \times 5'$ global grid of DTM2006.0 heights H^* to maximum degree $n_{max}^{DTM2006} =$
 305 2160 was computed using the spherical harmonic expansion [EGM-Team, 2008]

$$306 \quad H^* = \sum_{n=0}^{n_{max}^{DTM2006}} \sum_{m=0}^n (\overline{HC}_{nm}^* \cos m\lambda + \overline{HS}_{nm}^* \sin m\lambda) \overline{P}_{nm}(\cos \theta) \quad (1)$$

307 where \overline{HC}_{nm}^* and \overline{HS}_{nm}^* are the 4π -fully-normalized spherical harmonic coefficients of the
 308 DTM2006.0 database, $\overline{P}_{nm}(\cos \theta)$ are the 4π -fully-normalized associated Legendre functions
 309 of degree n and order m , and λ longitude and θ geocentric co-latitude of the computation
 310 point.

311 Second, the grid of DTM2006.0 H^* was converted to RET elevations H by
 312 transforming the ocean depths using [Rummel *et al.*, 1988; Wiczorek, 2007]

$$313 \quad H = \begin{cases} H^*(1 - \rho_w / \rho) & , H^* < 0 \\ H^* & , H^* \geq 0 \end{cases} \quad (2)$$

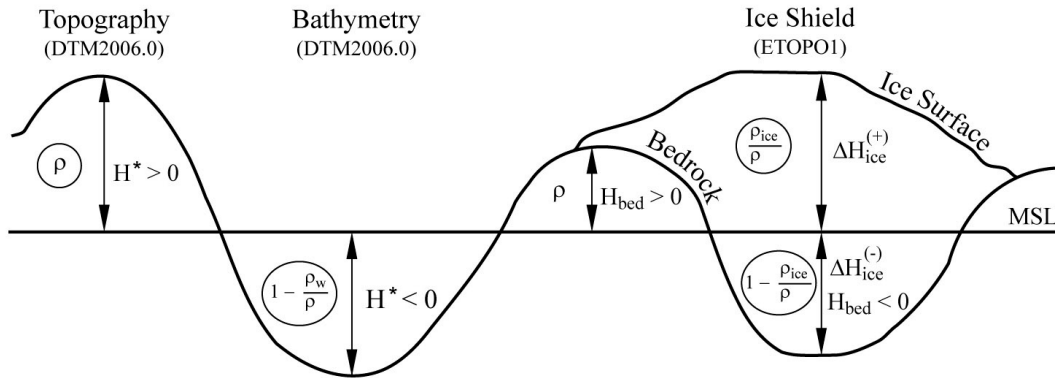
314 where ρ_w is the mean mass-density of ocean water (1030 kg m^{-3}) and ρ the mean mass-
 315 density of topographic rock (2670 kg m^{-3}). This reduction of ocean depths by factor
 316 $(1 - \rho_w / \rho) = 0.614$ compresses the ocean water into RET. Over Greenland and Antarctica
 317 DTM2006.0 heights represent the interface between ice and air, thus additional information
 318 on the bedrock underneath the ice shields is required to properly model the RET. Over these
 319 areas, DTM2006 was replaced by ETOPO1 (area-weight-averaged to a $5' \times 5'$ grid) which has
 320 been used to obtain RET heights through

$$321 \quad H = H_{bed} + \Delta H_{ice}^{(-)} \left(1 - \frac{\rho_{ice}}{\rho}\right) + \Delta H_{ice}^{(+)} \frac{\rho_{ice}}{\rho} \quad (3)$$

322 where H_{bed} is the bedrock height, ρ_{ice} is the mean mass-density of ice (927 kg m^{-3}) and
 323 $\Delta H_{ice}^{(+)}$ and $\Delta H_{ice}^{(-)}$ are the thicknesses of ice masses above and below mean sea level (MSL),
 324 cf. Fig 1. Equation (3) is valid for bedrock above MSL (e.g. $H_{bed} \geq 0$) and below MSL (e.g.
 325 $H_{bed} < 0$). The thickness $\Delta H_{ice}^{(+)}$ of ice masses above MSL are reduced by the factor $\rho_{ice} / \rho =$

326 0.347 and the thickness $\Delta H_{ice}^{(-)}$ of ice masses below MSL are reduced by the factor
 327 $(1 - \rho_{ice} / \rho) = 0.653$.

328



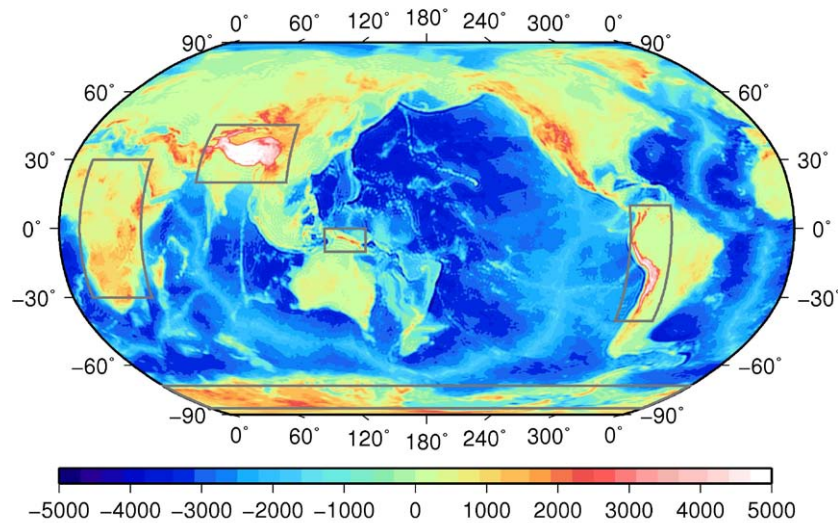
329

330 **Fig. 1.** Terrain types used to construct the rock-equivalent topography RET2011 heights.

331

332 Third, the $5' \times 5'$ grid of RET H was analyzed harmonically to yield spherical
 333 harmonic coefficients $\overline{HC}_{nm}, \overline{HS}_{nm}$ of RET2011. Though the GGM evaluation requires the
 334 $\overline{HC}_{nm}, \overline{HS}_{nm}$ coefficients only to degree 250, we derived $\overline{HC}_{nm}, \overline{HS}_{nm}$ to degree 360 which
 335 can be used for RET-based evaluation of future GGMs. Our spherical harmonic analysis is
 336 based on least-squares estimation of the harmonic coefficients [e.g., Colombo, 1981; Torge
 337 2001, p. 272]. Following this approach, a regular global grid of RET heights (symmetric to
 338 the equator) is used to develop grid elements along the same parallel into Fourier series in
 339 $\sin m\lambda$ and $\cos m\lambda$. Based on the Fourier series coefficients the 4pi-fully normalized
 340 spherical harmonic coefficients $\overline{HC}_{nm}, \overline{HS}_{nm}$ are obtained through least-squares estimation.
 341 RET2011 heights expanded to degree 250 (the maximum resolution of the second generation
 342 GOCE models) are shown in Figure 2.

343



344

345 **Fig. 2.** Earth's rock-equivalent topography RET2011 to spherical harmonic degree 250.

346 Robinson projection, units in metres. Grey boxes show evaluation regional used in Sect. 4

347 **3.3 Potential coefficients**

348 **3.3.1 Uncompensated RET**

349 The \overline{HC}_{nm} , \overline{HS}_{nm} coefficients of RET2011 were converted into gravitational potential
 350 spherical coefficients \overline{C}_{nm}^{RET} , \overline{S}_{nm}^{RET} using [Rummel et al., 1988; Kuhn and Featherstone, 2003]:
 351

$$352 \left\{ \begin{array}{l} \overline{C}_{nm}^{RET} \\ \overline{S}_{nm}^{RET} \end{array} \right\} = \frac{3}{2n+1} \cdot \frac{\rho}{\overline{\rho}} \left[\left\{ \begin{array}{l} \overline{HC1}_{nm} \\ \overline{HS1}_{nm} \end{array} \right\} + \frac{n+2}{2} \left\{ \begin{array}{l} \overline{HC2}_{nm} \\ \overline{HS2}_{nm} \end{array} \right\} + \frac{(n+2)(n+1)}{6} \left\{ \begin{array}{l} \overline{HC3}_{nm} \\ \overline{HS3}_{nm} \end{array} \right\} \right] \quad (4)$$

353 with $\overline{\rho}$ mean mass-density of Earth (5515 kg m⁻³) and ρ the mean mass-density of
 354 topographic rock (2670 kg m⁻³). $\overline{HC1}_{nm}$, $\overline{HS1}_{nm}$ are the spherical harmonic coefficients of the
 355 dimensionless surface function $H1 := H / R$ and obtained from

$$356 \begin{array}{l} \overline{HC1}_{nm} = \overline{HC}_{nm} / R \\ \overline{HS1}_{nm} = \overline{HS}_{nm} / R \end{array}, \quad (5)$$

357 where R is the equatorial Earth radius of 6378137 m [Torge, 2001]. $\overline{HC2}_{nm}$, $\overline{HS2}_{nm}$ denote
 358 the spherical harmonic coefficients of surface function $H2$

$$359 H2 := \left(\frac{H}{R} \right)^2 = \sum_{n=0}^{360} \sum_{m=0}^n (\overline{HC2}_{nm} \cos m\lambda + \overline{HS2}_{nm} \sin m\lambda) \overline{P}_{nm}(\cos \theta) \quad (6)$$

360 and $\overline{HC3}_{nm}$, $\overline{HS3}_{nm}$ are the coefficients of surface function $H3$

$$361 H3 := \left(\frac{H}{R} \right)^3 = \sum_{n=0}^{360} \sum_{m=0}^n (\overline{HC3}_{nm} \cos m\lambda + \overline{HS3}_{nm} \sin m\lambda) \overline{P}_{nm}(\cos \theta) \quad (7)$$

362 For evaluation of Eq. (4), $\overline{HC1}_{nm}$, $\overline{HS1}_{nm}$ are readily available from Eq. (5), while two
 363 additional spherical harmonic analyses are needed to derive the coefficients $\overline{HC2}_{nm}$, $\overline{HS2}_{nm}$
 364 and $\overline{HC3}_{nm}$, $\overline{HS3}_{nm}$ of the surface functions $H2$ and $H3$, respectively. The surface
 365 functions $H2$ and $H3$ are computed as a function of H (Eqs. 6 and 7) after the H were
 366 synthesized on a high-resolution grid using

$$367 H = \sum_{n=0}^{360} \sum_{m=0}^n (\overline{HC}_{nm} \cos m\lambda + \overline{HS}_{nm} \sin m\lambda) \overline{P}_{nm}(\cos \theta) \quad (8)$$

368
 369 Equation (4) is a series expansion to third-order of H , which is obtained by replacing
 370 the inverse distance in Newton's integral through a series of Legendre polynomials [e.g.,
 371 Heiskanen and Moritz, 1967, p. 32]. A first-order expansion delivers well above 90% of the
 372 overall topography-implied gravity signal [cf. Novák and Grafarend 2005, Fig. 3]. With any
 373 additional term, topography-implied signal captured by the \overline{C}_{nm}^{RET} , \overline{S}_{nm}^{RET} potential coefficients
 374 comes closer to 100% and the contribution of every additional term is smaller than the
 375 previous [Wieczorek, 2007]. According to Wieczorek [2007, Fig. 9 ibid.], the maximum
 376 (truncation) error of a third-order expansion is a few mGal, and the average root mean square

377 (RMS) error is well below the mGal-level. Given that the global RMS gravity signal strength
 378 is ~35 mGal [*EGM-Team, 2008*], the third-order expansion appears sufficient.

379

380 3.3.2 Airy-Heiskanen compensation

381 In the A/H model, a lighter lithosphere is assumed to float on a denser mantle, and
 382 isostatic compensation is assumed to take place locally in vertical columns of equal mass-
 383 density [e.g., *Heiskanen and Moritz, 1967; Watts, 2001, Torge, 2001*]. As a consequence, the
 384 depth of the sub-surface compensation mass is directly related to the height of the topography
 385 (“local compensation”), and the spatial resolution of the A/H compensation model is
 386 [formally] identical to the resolution of the topographic model used. The potential
 387 coefficients of the A/H-compensated RET are computed from a series expansion to third-
 388 order [*Rummel et al., 1988, Eq. 24*]

$$\begin{aligned}
 \left\{ \begin{array}{l} \overline{C}_{nm}^{A/H} \\ \overline{S}_{nm}^{A/H} \end{array} \right\} &= \frac{3}{2n+1} \cdot \frac{\rho}{\rho} \left[\left[1 - \left(\frac{R-T}{R} \right)^n \right] \left\{ \begin{array}{l} \overline{HC1}_{nm} \\ \overline{HS1}_{nm} \end{array} \right\} + \frac{n+2}{2} \left[1 + \frac{\rho}{\rho_m - \rho} \left(\frac{R-T}{R} \right)^{n-3} \right] \left\{ \begin{array}{l} \overline{HC2}_{nm} \\ \overline{HS2}_{nm} \end{array} \right\} \right. \\
 &\quad \left. + \frac{(n+2)(n+1)}{6} \left[1 - \left(\frac{\rho}{\rho_m - \rho} \right)^2 \left(\frac{R-T}{R} \right)^{n-6} \right] \left\{ \begin{array}{l} \overline{HC3}_{nm} \\ \overline{HS3}_{nm} \end{array} \right\} \right] \quad (9)
 \end{aligned}$$

390 where T denotes the mean depth of compensation and ρ_m the mass-density of the mantle.
 391 Here we use $T = 30$ km and $\rho_m = 3270$ kg m⁻³ [*Torge, 2001, p. 341*]. The potential
 392 coefficients $\overline{C}_{nm}^{A/H}, \overline{S}_{nm}^{A/H}$ contain the effect both of the topography and of the A/H-
 393 compensation masses. The practical computation of the $\overline{C}_{nm}^{A/H}, \overline{S}_{nm}^{A/H}$ is straightforward as the
 394 required sets of potential coefficients of the uncompensated RET ($\overline{HC1}_{nm}, \overline{HS1}_{nm}$,
 395 $\overline{HC2}_{nm}, \overline{HS2}_{nm}$ and $\overline{HC3}_{nm}, \overline{HS3}_{nm}$) are readily available from Sect. 3.3.1. We acknowledge
 396 that the value of $T = 30$ km is not valid for oceans, so a combination is trialed later (Sect
 397 3.3.4).

398

399 3.3.3 Pratt/Hayford compensation

400

401 The P/H isostatic compensation uses a constant depth of compensation along with
 402 laterally-varying mass-densities of vertical columns [e.g., *Watts, 2001, Torge, 2001*]. A
 403 compact formulation of the potential coefficients $\overline{C}_{nm}^{P/H}, \overline{S}_{nm}^{P/H}$ of the P/H-compensated
 404 topography is given by *Göttl and Rummel [2009]* as:

$$\begin{aligned}
 \left\{ \begin{array}{l} \overline{C}_{nm}^{P/H} \\ \overline{S}_{nm}^{P/H} \end{array} \right\} &= \frac{3}{2n+1} \cdot \frac{\rho}{\rho} \left[\left\{ \begin{array}{l} \overline{hC1}_{nm} \\ \overline{hS1}_{nm} \end{array} \right\} + \frac{n+2}{2} \left\{ \begin{array}{l} \overline{hC2}_{nm} \\ \overline{hS2}_{nm} \end{array} \right\} + \frac{(n+2)(n+1)}{6} \left\{ \begin{array}{l} \overline{hC3}_{nm} \\ \overline{hS3}_{nm} \end{array} \right\} \right] \\
 &\quad + \frac{3}{(2n+1)(n+3)} \frac{\rho}{\rho} \left[1 - \left(\frac{R-D}{R} \right)^{n+3} \right] \left\{ \begin{array}{l} \overline{\rho C}_{nm} \\ \overline{\rho S}_{nm} \end{array} \right\} \quad (10)
 \end{aligned}$$

405

406 where D is the depth of compensation [here 100 km], $\bar{\rho}$ mean mass-density of Earth (5515
407 kg m⁻³), ρ the mean mass-density of topographic rock (2670 kg m⁻³). The $\overline{hC1_{nm}}, \overline{hS1_{nm}},$
408 $\overline{hC2_{nm}}, \overline{hS2_{nm}},$ and $\overline{hC3_{nm}}, \overline{hS3_{nm}}$ are the spherical harmonic coefficients of the
409 dimensionless height function h/R times the dimensionless density function ρ_i/ρ and
410 $\overline{\rho C_{nm}}, \overline{\rho S_{nm}}$ are the spherical harmonic coefficients of the dimensionless density function
411 ρ_i/ρ [Mladek, 2006, p 74]:

$$413 \quad h1 := \left(\frac{h}{R} \frac{\rho_i}{\rho} \right) = \sum_{n=0}^{360} \sum_{m=0}^n (\overline{hC1_{nm}} \cos m\lambda + \overline{hS1_{nm}} \sin m\lambda) \overline{P_{nm}}(\cos \theta) \quad (11)$$

$$414 \quad h2 := \left(\frac{h}{R} \frac{\rho_i}{\rho} \right)^2 = \sum_{n=0}^{360} \sum_{m=0}^n (\overline{hC2_{nm}} \cos m\lambda + \overline{hS2_{nm}} \sin m\lambda) \overline{P_{nm}}(\cos \theta) \quad (12)$$

$$415 \quad h3 := \left(\frac{h}{R} \frac{\rho_i}{\rho} \right)^3 = \sum_{n=0}^{360} \sum_{m=0}^n (\overline{hC3_{nm}} \cos m\lambda + \overline{hS3_{nm}} \sin m\lambda) \overline{P_{nm}}(\cos \theta) \quad (13)$$

$$417 \quad \rho1 := \frac{\rho_i}{\rho} = \sum_{n=0}^{360} \sum_{m=0}^n (\overline{\rho C_{nm}} \cos m\lambda + \overline{\rho S_{nm}} \sin m\lambda) \overline{P_{nm}}(\cos \theta) \quad (14)$$

418
419 Variable h denotes the equivalent rock heights of the P/H model and ρ_i are the [individual]
420 mass-densities of the vertical columns. According to *Göttl and Rummel* [2009] the P/H
421 equivalent rock heights h are determined via:

$$423 \quad h = \begin{cases} H & , H^* \geq 0 \\ \left(\frac{\rho(R+H^*)^3[-R^3+(R-D)^3] - \rho_w(R-D)^3[-R^3+(R+H^*)^3]}{\rho_w[R^3-(R+H^*)^3] - \rho[R^3-(R-D)^3]} \right)^{1/3} - R & , H^* < 0 \end{cases} \quad (15)$$

424 where H are the RET2011 heights [from Eqs.(2) and (3)], H^* are the DTM2006 bathymetric
425 depths/topographic heights, and ρ_w is the mean mass-density of ocean water (1030 kg m⁻³).
426 Equation (15) is the formulation of the P/H equilibrium condition over the oceans [*Göttl and*
427 *Rummel* 2009, p 1253]. Over land areas, RET2011 heights H (topography or ice) and h are
428 identical, while H and h are different over the oceans. Note that *Göttl and Rummel* [2009]
429 used a different sign convention for bathymetric depths. The individual mass-densities ρ_i are
430 obtained from

$$431 \quad \rho_i = \rho \left(\frac{R^3 - (R-D)^3}{(R+h)^3 - (R-D)^3} \right) . \quad (16)$$

432 For the practical computation of the P/H-compensated rock-equivalent topography, we back-
433 converted the RET2011 heights to bathymetric depths H^* over the oceans, and applied Eq.
434 (15) to obtain rock-equivalent heights h , consistent with the P/H equilibrium condition. We

435 then computed the individual mass-densities ρ_i [Eq. (16)] of the $5' \times 5'$ grid, and analyzed
 436 harmonically the dimensionless linear, squared and cubic height functions $h1, h2, h3$ [Eq.
 437 (11)-(13)]. A further harmonic analysis of the $5' \times 5'$ grid of ρ^1 [Eq. (14)] yielded the
 438 $\overline{\rho C_{nm}}, \overline{\rho S_{nm}}$ coefficients required to finally obtain the $\overline{C_{nm}^{P/H}}, \overline{S_{nm}^{P/H}}$ potential coefficients of the
 439 P/H compensated rock-equivalent topography [Eq. (10)]. The potential coefficients $\overline{C_{nm}^{P/H}},$
 440 $\overline{S_{nm}^{P/H}}$ contain the effect both of the topography and of the P/H-compensation masses.

441

442 3.3.4 Combined A/H and P/H compensation model

443 *Göttl and Rummel* [2009] analyzed A/H and P/H compensated gravity anomalies over land
 444 and ocean areas and found that the A/H is better suited than P/H to model the isostatic
 445 compensation of large mountain chains, while their analysis suggests that P/H is a better
 446 approximate description of isostasy over deep ocean trenches. We therefore combine the
 447 classical A/H [Sect. 3.3.2] and P/H [Sect. 3.3.3] hypotheses, by using A/H over land areas
 448 and P/H over the oceans. A/H and P/H are combined in the spatial domain by using gravity
 449 implied by the P/H-compensated topography at points where $H^* < 0$ and the A/H-
 450 compensated topography elsewhere, see also *Wild and Heck* [2005]; *Makhloof* [2007] who
 451 used the same combination strategy. “By this mixture, one of the drawbacks of the original
 452 Airy-Heiskanen model – the fact that the antiroots may rise above the ocean bottom in deep
 453 sea trough areas – can be avoided.” [Wild and Heck 2005, p233].

454

455 3.4 Gravity computations

456 Gravity disturbances δg^{GGM} from each GGM were computed at points specified by radius $r,$
 457 longitude λ and geocentric co-latitude θ from the spherical harmonic coefficients
 458 $\overline{C_{nm}^{GGM}}, \overline{S_{nm}^{GGM}}$ of the various GOCE GGMs via [*Heiskanen and Moritz*, 1967; *Torge*, 2001]

$$459 \quad \delta g^{GGM} = \frac{GM^{GGM}}{r^2} \sum_{n=n_1}^{n_2} \left(\frac{a^{GGM}}{r} \right)^n (n+1) \sum_{m=0}^n (\overline{C_{nm}^{GGM}} \cos m\lambda + \overline{S_{nm}^{GGM}} \sin m\lambda) \overline{P}_{nm}(\cos \theta) \quad (17)$$

460 where a_{GGM} (model scale factor) and GM_{GGM} (gravitational constant times Earth’s mass) are
 461 the model-specific constants, and n_1, n_2 are the minimum and maximum harmonic degree,
 462 respectively, of the spectral band being examined. Similarly, the RET potential coefficients
 463 $\overline{C_{nm}^{RET}}, \overline{S_{nm}^{RET}}$ are evaluated to give gravity disturbances δg^{RET} implied by the uncompensated
 464 RET.

$$465 \quad \delta g^{RET} = \frac{GM}{r^2} \sum_{n=n_1}^{n_2} \left(\frac{a}{r} \right)^n (n+1) \sum_{m=0}^n (\overline{C_{nm}^{RET}} \cos m\lambda + \overline{S_{nm}^{RET}} \sin m\lambda) \overline{P}_{nm}(\cos \theta) \quad (18)$$

466 where $GM = GM^{GGM} = 3.986004415 \times 10^{14} \text{ m}^3 \text{ s}^{-2}$ for all seven GGMs assessed (Table 1).
 467 Accordingly, evaluating Eq. (18) with the $\overline{C_{nm}^{A/H}}, \overline{S_{nm}^{A/H}}, \overline{C_{nm}^{P/H}}, \overline{S_{nm}^{P/H}}$ gives gravity disturbances
 468 $\delta g^{A/H}$ ($\delta g^{P/H}$) of the A/H-compensated and P/H-compensated topography, respectively. The
 469 gravity $\delta g^{A/H-P/H}$ implied by the combined A/H-P/H model is obtained by using $\delta g^{P/H}$ over

470 the oceans and $\delta g^{A/H}$ elsewhere. Hereafter, we use the general term “gravity” for δg^{GGM} ,
 471 δg^{RET} and $\delta g^{A/H}$, $\delta g^{P/H}$ and $\delta g^{A/H-P/H}$ from Eqs. (17) and (18).

472 Equations (17) and (18) were evaluated with the harmonic_synth software [Holmes
 473 and Pavlis, 2008] on the surface of an authalic sphere with radius $r = R = 6378137$ m. This
 474 sets the attenuation factor $(a/r)^n$ in Eq. (18) to unity, while $(a^{GGM}/R)^n$ is very close to
 475 unity in Eq. (17). The $(a^{GGM}/r)^n$ ranges between 0.999973 and 1, because $a^{GGM} - r < 1$ m
 476 for all seven GGMs assessed and the smallest possible value of $(a^{GGM}/r)^n$ is 0.999973 (for n
 477 = 250 and $a^{GGM} = 6378136.3$ m). As a consequence, the attenuation factors only affect our
 478 evaluation results by less than 0.003%, which is negligible.

479

480 **4. Analyses and results**

481 **4.1 Evaluation criteria**

482 **4.1.1 Correlation coefficients and reduction rates**

483 We computed $10' \times 10'$ grids of GGM gravity for each GGM in Table 1 over a series of two-
 484 degree spectral bands $[n, n+1]$, starting from $[2, 3]$ up to $[n_{max}-1, n_{max}]$ the model’s maximum
 485 degree n_{max} , and then compared these against gravity implied by the (i) uncompensated RET,
 486 (ii) A/H-compensated RET, (iii) P/H-compensated RET and (iv) A/H-P/H combined
 487 compensated RET in the same bands in the spatial domain.

488 To evaluate the GGM’s spectral content as a function of degree we use cross-
 489 correlation coefficients (CCs) between δg^{GGM} and δg^{RET} , δg^{GGM} and $\delta g^{A/H}$, δg^{GGM} and
 490 $\delta g^{P/H}$, and δg^{GGM} and $\delta g^{A/H-P/H}$, respectively. CCs between topography and gravity have
 491 been used previously, e.g., by Rapp [1982], Rummel *et al.*, [1988] and Wieczorek [2007],
 492 amongst many others. We also use a new indicator called reduction rates (RRs), given by:

$$493 \quad RR = 100\% \cdot \left(1 - \frac{RMS(\delta g^{REF} - \delta g^{GGM})}{RMS(\delta g^{REF})} \right) \quad (19)$$

494 where RMS is the root mean square of the δg^{REF} and the differences $(\delta g^{REF} - \delta g^{GGM})$,
 495 respectively, and δg^{REF} is the reference signal, which can either be gravity implied by the
 496 uncompensated topography (δg^{RET}), by the A/H-compensated topography ($\delta g^{A/H}$), the P/H-
 497 compensated topography ($\delta g^{P/H}$), or the combined A/H-P/H-compensated topography
 498 $\delta g^{A/H-P/H}$.

499 Reduction rates (RRs) quantify the extent to which the signal strength of δg^{REF} is
 500 reduced (‘explained’) by the model gravity δg^{GGM} or, in other words, the strength of δg^{REF}
 501 signals captured by the δg^{GGM} . Moderate positive RRs (say about 30% to 50%) indicate
 502 considerable topography-generated gravity signals are captured by the GGM, whereas RRs
 503 near or below 0% show that the GGM signal is unrelated to the topography. Smaller, but
 504 positive, RRs (say about 10% to 20%) indicate that the GOCE model contains TIG signals
 505 δg^{REF} to some, but limited, extent. RRs close to 80-90 % indicate that the GGM signal is
 506 almost entirely generated by the modeled topography. However, given the presence of

507 unmodeled mass-density anomalies in the real topography and the Earth's interior, such
 508 values do not occur at the spatial scales resolved by GOCE (see Sects 4.2 and 4.3). From Eq.
 509 (19), RRs cannot exceed 100%.

510 Moderate positive RRs always correspond to large positive CCs between δg^{REF} and
 511 δg^{GGM} . Conversely, a large positive CC between δg^{REF} and δg^{GGM} does not necessarily
 512 correspond to a large RR. In cases where the model is underpowered near the model
 513 resolution (due to gravity attenuation at satellite height), we consider it possible that δg^{REF}
 514 and δg^{GGM} are strongly correlated (the gravity highs and lows appear at the same locations),
 515 but the δg^{GGM} RMS signal strength is smaller than implied by the topography δg^{REF} .
 516 Despite larger CCs, RRs will then be low, thus better indicating the deteriorating quality of
 517 the model. We have tested RRs extensively using both the δg^{RET} , $\delta g^{A/H}$, $\delta g^{P/H}$ and
 518 $\delta g^{A/H-P/H}$ as reference δg^{REF} in Eq. (19). As a prerequisite for moderate positive RRs, the
 519 RMS signal strength of δg^{REF} has to be similar (or larger) than that of the observed gravity
 520 δg^{GGM} . Otherwise, the RMS ($\delta g^{REF} - \delta g^{GGM}$) will exceed the RMS(δg^{REF}), failing to
 521 indicate topography-generated signals in the GGM.

522

523 **4.1.2 Effective and formal model resolution**

524 Degree-wise comparisons between quantities derived from spherical harmonic models
 525 are always subject to oscillations [e.g., *Rapp*, 1982; *Rummel et al.*, 1988; *Wieczorek*, 2007;
 526 *Gruber et al.*, 2011]. Because these oscillations also propagate into quality indicators (be it
 527 CCs, RRs or other indicators), and because most of the GGMs contain topographic signals
 528 over their entire spectrum, it is generally difficult to discriminate the maximum harmonic
 529 degree upon which the GGMs deliver full (i.e., not affected by attenuation) information on
 530 Earth's gravity field (also see *Gruber et al.*, [2011]; *Hirt et al.*, [2011]). We found that
 531 neither the harmonic degree where the RRs are maximum nor constant thresholds (e.g., 20 %)
 532 are informative numerical criteria because these oscillations vary from region to region. As a
 533 compromise, we use the following simple numerical threshold

$$534 \quad t = f \times \bar{r}, \quad (20)$$

535 where $f = 0.85$ and \bar{r} is the GGMs average RR in band 100 to 175 over the region under
 536 investigation.

537 What we will term the *effective resolution* is the smallest harmonic degree (but larger
 538 than 150) where the GGM's RR falls below our threshold criterion (Eq. 20). The effective
 539 resolution indicates the degree where the GGMs seem to possess almost full spectral power.
 540 Opposed to this, the *formal resolution* is the maximum expansion degree of the GGMs in
 541 Table 1. We acknowledge that the criterion in Eq. (20) is somewhat arbitrary because the
 542 choice of factor f influences the threshold and thus the interpreted effective resolution.
 543 However, the use of this criterion suppresses the influence of the oscillations (Sections 4.2
 544 and 4.3) on the choice of effective resolution because the same criterion applies to all GGMs
 545 and they are being compared in a relative manner.

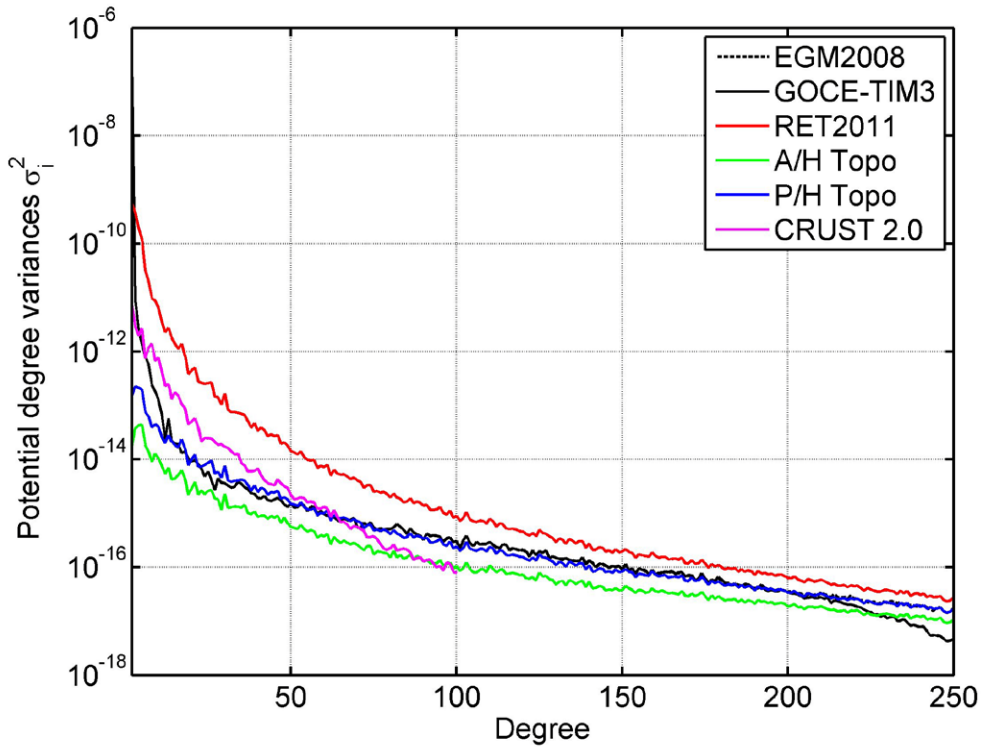
546

547 **4.2 Preliminary comparisons**

548 To initially analyze the spectral properties of our data sets, we have computed
 549 [dimensionless] potential degree variances σ_n [e.g., *Rapp*, 1982; *Rummel et al.*, 1988]

$$550 \quad \sigma_n = \sum_{m=1}^n \overline{C}_{nm}^2 + \overline{S}_{nm}^2 \quad (21)$$

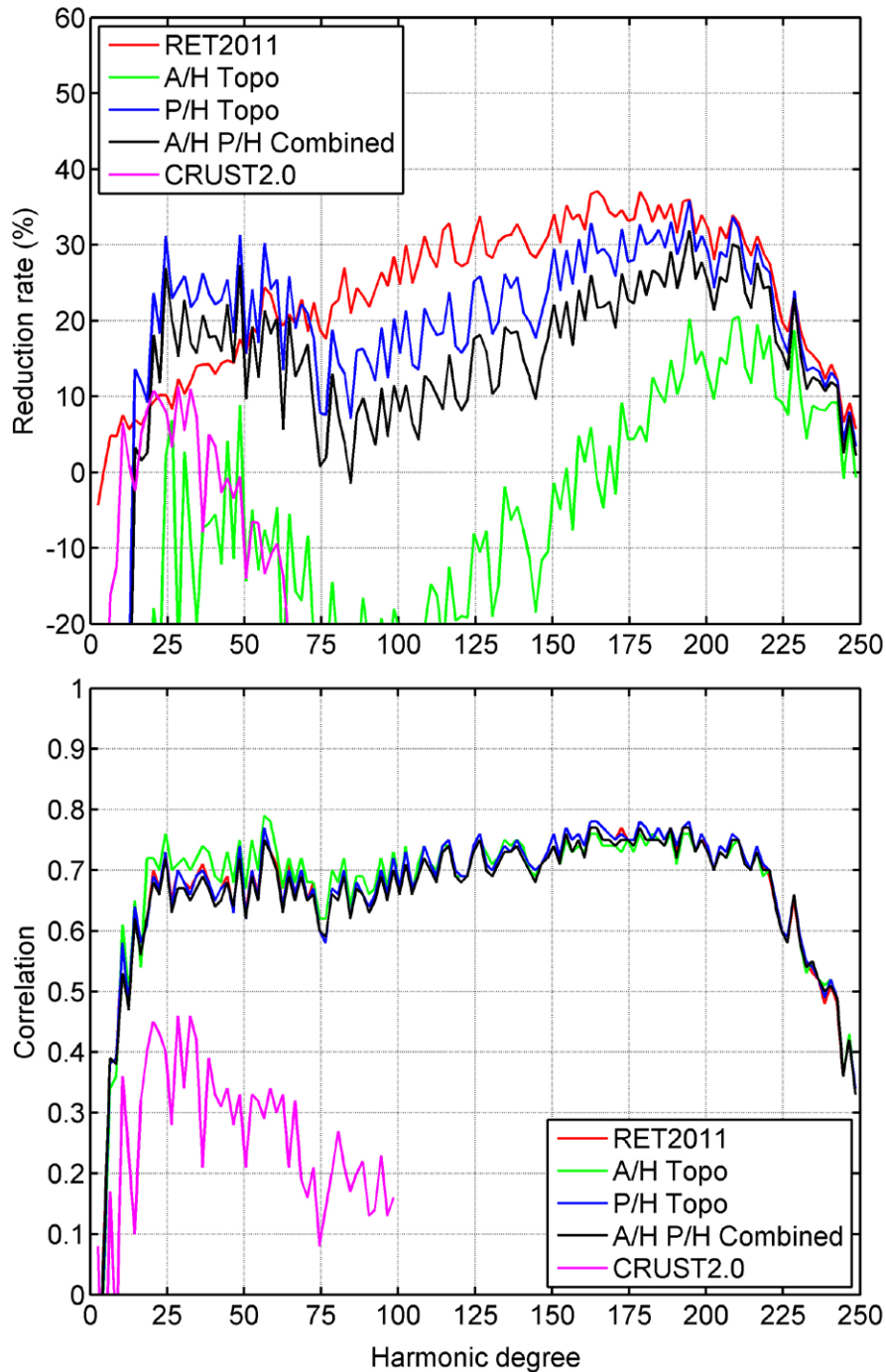
551 where n is the degree, m the order and \overline{C}_{nm} \overline{S}_{nm} are the spherical harmonic coefficients of the
 552 GGMs, of the uncompensated RET, or of the A/H- or P/H-compensated topography. From
 553 Fig. 3, the (uncompensated) RET significantly exceeds the spectral power of Earth’s
 554 observed gravity field, as represented through EGM2008 and GOCE-TIM3. This behavior
 555 (e.g., *Rummel et al.* [1988, Fig. 2]; *Watts*, [2001, p 416]) shows that the gravitational
 556 attraction of isostatic compensation masses and other mass-density anomalies in the Earth’s
 557 interior “compete” with the attraction of Earth’s uncompensated topography, most
 558 significantly at long- and medium wavelengths. The A/H compensation model diminishes
 559 the spectral power of the uncompensated topography to a level well below that of Earth’s
 560 observed gravity field (see also *Rummel et al.* [1988]). Opposed to this, the spectral power of
 561 the P/H-compensated topography is very similar to that of Earth’s observed gravity field,
 562 which is in agreement with *Makhloof* [2007, p102].
 563



564 **Fig. 3.** Dimensionless degree variances of selected GGMs and topographic/isostatic models.
 565
 566

567 To gain some insight into the effectiveness of our topography and compensation
 568 variants to indicate topography/isostasy-implied signals in the GOCE gravity fields, we
 569 compared gravity δg^{GGM} from the highest-resolution space-collected GGM GOCE-TIM3
 570 with δg^{RET} , $\delta g^{A/H}$ and $\delta g^{P/H}$, and with the combined $\delta g^{AH/PH}$ as a function of the

571 spherical harmonic degree over a near-global area ($-83.3^{\circ} \leq \varphi \leq 83.3^{\circ}$ and $-180^{\circ} \leq \lambda \leq 180^{\circ}$).
 572 From Fig. 4 (top), RRs using the uncompensated RET2011 as a reference are generally larger
 573 than RRs using compensated RET. RRs using $\delta g^{P/H}$ as a reference are largest at the long
 574 spatial scales, at the 20% level at medium scales and comparable to that of RET2011 beyond
 575 degree 200. From Fig. 4 (top), P/H appears to better describe isostasy globally at long- and
 576 medium scales than A/H. For the combined A/H-P/H model, RRs are larger than of A/H and
 577 below those of the P/H.



578
 579 **Fig. 4.** Reduction rates (top) and cross-correlation coefficients (bottom) between GOCE-
 580 TIM3 and various topographic/isostatic models as a function of harmonic degree n .
 581 Evaluation area is $-83.3^{\circ} \leq \varphi \leq 83.3^{\circ}$ and $-180^{\circ} \leq \lambda \leq 180^{\circ}$.

582 The CCs for all three topographic/isostatic models agree reasonably well over all
583 harmonic degrees (Fig. 4 bottom), and thus do not allow discrimination between the different
584 topographic/isostatic models. Only RRs are capable of discriminating between the
585 topographic/isostatic models (Fig. 4 top), and additionally indicate the increasing relevance
586 of topography-generated signals in the observed gravity field (seen by the steadily increasing
587 RRs up to degree ~ 200). Given that RRs require a reference signal δg^{REF} of sufficient
588 spectral power (see Sect. 4.1.1 and Fig. 3), it becomes clear that the underpowered A/H
589 compensated topography does not serve well as reference signal at long and medium spatial
590 scales (seen by the very low or negative RRs for A/H in Fig. 4 top). Focusing on spatial
591 scales less than ~ 100 km (that is, beyond harmonic degree 200), CCs and RRs indicate –
592 irrespective of using uncompensated or compensated topography – a declining amount of
593 topography-generated gravity signals. However, neither the CCs nor RRs indicate that the
594 agreement of GOCE-measured gravity with Earth’s topography improves over RET2011
595 when employing the isostatic compensation models at ~ 100 km spatial scales.

596 Neglecting the isostatic compensation masses, the uncompensated RET2011 should
597 theoretically be the poorer representation of Earth’s topography/isostasy, while adding
598 isostatic compensation effects to RET2011 should be a theoretically better representation.
599 However, the observation that the isostatic models do not improve the agreement over
600 RET2011-only at medium and short spatial scales suggests that none of the isostatic models
601 included here is a very suitable representation of compensating masses.

602 For comparison purposes, the Crust.2.0 lithosphere model has been tested as an
603 “observation-based” global description of crustal thickness (potential coefficients are from
604 *Kuhn and Featherstone*, [2003], derived through spherical harmonic analysis of the upper-
605 middle and lower crustal layers as well as the crust-mantle boundary aka Moho). From Fig.
606 3, Crust 2.0’s spectral power ranges between RET and Earth’s observed gravity up to
607 harmonic degree ~ 50 , and declines rapidly at medium wavelengths. Comparison among
608 Crust 2.0-implied gravity and the GOCE-observed gravity field (Fig. 4) shows generally low
609 CCs (less than +0.5), with the RRs indicating some crustal signals captured by GOCE
610 (through GPS-based orbit determination) between degrees 10 and 40. The Crust.2.0-implied
611 gravity field bears little resemblance to the Earth’s gravity field, and fails to deliver
612 meaningful information beyond degree ~ 40 , so is unusable to provide a feedback on the
613 GOCE-measured short-scale gravity field.

614 We acknowledge that the A/H and P/H isostatic compensation models reduce the
615 differences between Earth’s observed gravity field and gravity effects implied by the
616 uncompensated topography regionally to some extent (cf. *Watts* [2011], Fig. 1; *Göttl and*
617 *Rummel* [2009], p 1255). However, From Fig. 4 it is evident that the A/H and P/H models –
618 along with the evaluation methodology applied here – fail to improve the agreement between
619 GOCE and the uncompensated topography globally.

620 The observation that the A/H and P/H compensation models do not improve the
621 agreement does not necessarily imply that isostatic compensation is not present at all at short,
622 say ~ 100 km, scales. It only implies that the classical hypotheses are of limited use to
623 accurately model local isostatic compensation globally. We conclude that the A/H and P/H
624 and combined compensation models are not better suited than the uncompensated topography

625 (RET2011) to study the resolution of the new GOCE gravity fields. As a consequence, we
626 use the uncompensated topography δg^{RET} as reference δg^{REF} in our global and regional
627 comparisons in the sequel.

628

629 **4.3 Near-global comparisons with RET2011**

630 The polar regions ($|\varphi| > 83.3^\circ$) that GOCE cannot fly over due to its orbital inclination
631 of 96.7° are excluded from the following comparisons. Figure 5 shows the RRs (top) and
632 CCs (bottom) between $10' \times 10'$ near-global grids of δg^{GGM} and δg^{RET} as a function of degree
633 for each GGM (cf. Table 1). RRs increase to $\sim 35\%$ up to degree ~ 150 , almost identically for
634 all models, showing the increasing strength of topographic gravitational signals captured by
635 the GGMs. Up to degree ~ 150 , neither the CCs nor RRs differ markedly for any of the
636 GGMs. Hence, at low- and medium-frequencies, both indicators are unable to discriminate
637 among their performance.

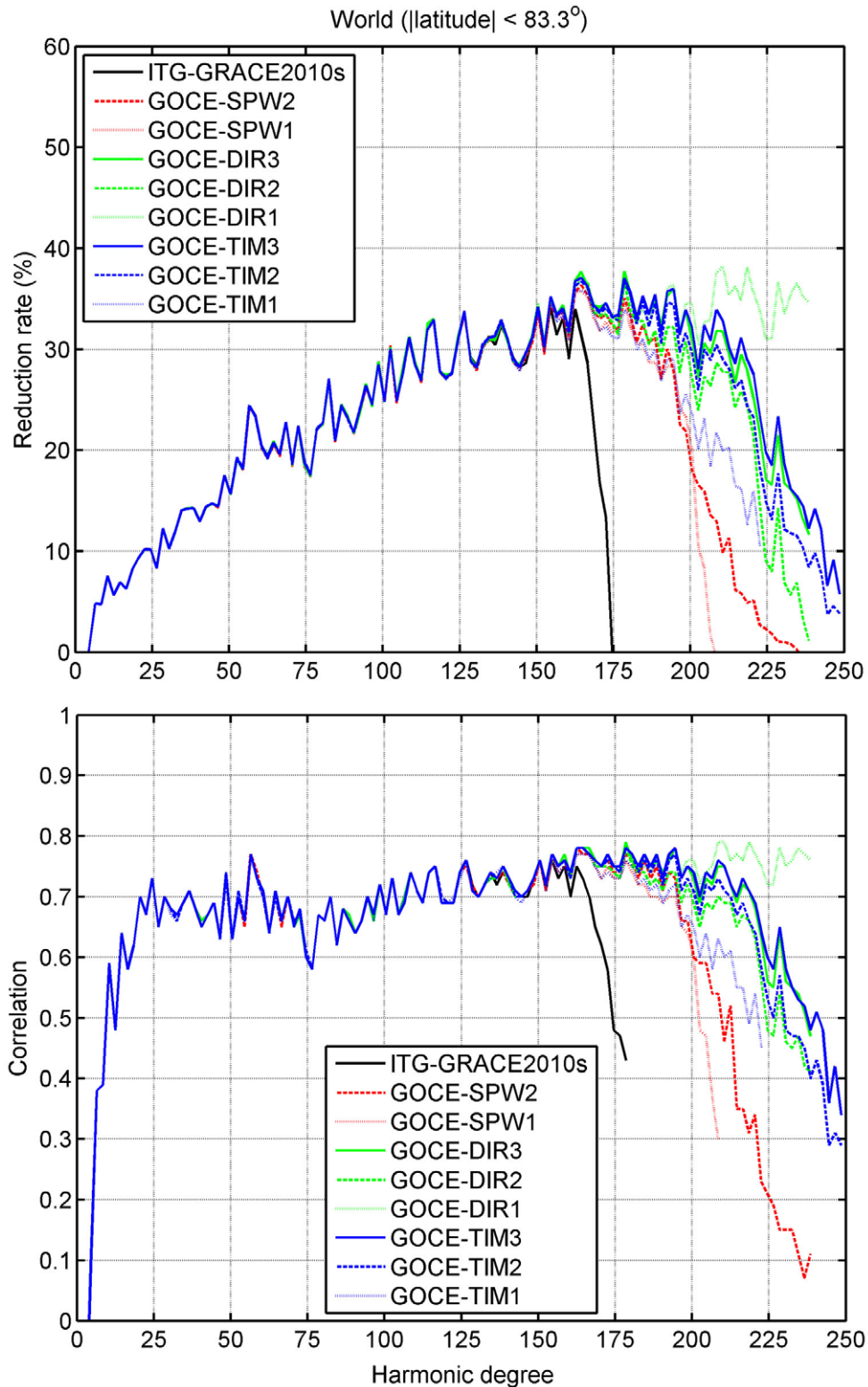
638 Beyond degree ~ 150 , RRs and CCs start to diverge for all GGMs. This now allows
639 for discrimination among their short-scale agreement with topography-generated gravity
640 signals. The topography is considered to be the dominant source of short-scale gravity field
641 signals [e.g., *Forsberg and Tscherning*, 1981; *Pavlis et al.*, 2007; *Hirt et al.*, 2010b, 2011],
642 which is why an improved agreement between measured and topography-generated gravity
643 can be expected with increasing harmonic degree n . Therefore, the drop in RRs and CCs
644 (Fig. 5) indicate that the GGMs lose spectral power, i.e., are increasingly unable to capture
645 the topography-implied gravity signal. From Fig. 5, we infer

- 646 • ITG-GRACE2010s starts losing topography-generated signals near degree ~ 160 ,
- 647 • All GOCE-GGMs capture topographic signals well up to degree ~ 175 , with RRs close
648 to $\sim 40\%$ and CCs near $+0.75$,
- 649 • The first-generation GOCE-GGMs SPW1 and TIM1 show a very similar decline in
650 signal between degrees ~ 180 and ~ 200 , whilst the second- and third-generation
651 GOCE GGMs start losing topography signals between degrees ~ 200 and ~ 220 .

652

653 Furthermore,

- 654 • The performance curves of DIR2 and TIM2, and of DIR3 and TIM3 are very close
655 together, separated from SPW2 by a spectral difference of ~ 15 harmonic degrees.
- 656 • The third-generation DIR3 and TIM3 improve over the second generation DIR2 and
657 TIM2 in the spectral band of ~ 200 to ~ 240 , where the RRs of the third-generation
658 models are by $\sim 5\%$ larger than of those of the second generation. TIM3 shows the
659 best agreement with gravity generated by the uncompensated topography.
- 660 • Even near or at their formal resolution (cf. Table 1), the GOCE GGMs exhibit
661 positive RRs, showing the sensitivity of GOCE for short-scale topography signals,
662 beyond degree ~ 200 , albeit strongly attenuated. The highest sensitivity for short-scale
663 gravity recovery is visible for DIR3 and TIM3 (positive RRs up to degrees ~ 240 - 250).
- 664 • DIR1 shows a good agreement with the topography up to its formal resolution of
665 degree 240, but this is because of its high-frequency augmentation with terrestrial data
666 (Table 1).



667
 668 **Fig. 5.** Reduction rates and cross-correlation coefficients between RET2011 and GGM
 669 gravity as a function of degree n . Evaluation area is $-83.3^\circ \leq \varphi \leq 83.3^\circ$ and $-180^\circ \leq \lambda \leq 180^\circ$.
 670

671 The effective GGM resolutions, computed from the criterion in Eq. (20), are reported
 672 in Table 2. TIM1 and SPW1 seem to capture most of the topography-generated gravity
 673 signals to degree ~ 195 , which is somewhat larger than assessments based on ground-truth

674 gravity field functionals [cf. *Gruber et al.*, 2011, *Hirt et al.*, 2011]. The second- and third-
675 generation GOCE GGMs possess almost full power to degree ~ 200 and ~ 220 respectively,
676 which is an improvement over the first-generation GOCE GGMs and over ITG-
677 GRACE2010s from the pre-GOCE-era. From Fig. 3, the GOCE TIM3 and EGM2008 degree
678 variances are in close agreement up to degree ~ 210 - 220 , which corroborates our results from
679 Fig. 5. It should be stressed here that the GGMs spectral content extends beyond their
680 effective resolution; however, gravity field signals are found to be increasingly attenuated.
681 This is within expectation, given that satellite gravimetry cannot sense the high-frequency
682 gravity field because of the decaying gravity signals at satellite altitude [e.g. *Kaula*, 1966].

683 The relation between GOCE- and topography-implied gravity (Fig. 5) poses the
684 question why CCs are not greater than $\sim +0.7$, and only about $\sim 35\%$ of GOCE-measured
685 gravity is explained by RET at scales of ~ 100 km (regionally, these values can be higher, see
686 Section 4.2). *Wieczorek* [2007] analyzed the correlation between gravity (from a GRACE-
687 based GGM) and (rock-equivalent) topography, yielding CCs at a similar level of $+0.7$,
688 which corroborates our results using RET2011. Importantly, CCs are not higher when
689 applying Crust 2.0, or A/H and P/H compensation models, as was shown in Fig. 4. We
690 therefore infer that topography-implied gravity (as well as those implied by the hypothesis-
691 based compensated topography, cf. Sect 4.1) globally explains GOCE-captured gravity to
692 some, but still limited, extent at spatial scales of ~ 100 km, and significant crustal mass-
693 density anomalies exist that superimpose the RET2011-generated signals, and those of the
694 A/H and P/H-compensated topography. Given that the topography/isostasy models used here
695 fail to explain the majority of GOCE-captured gravity signals, there is some potential to
696 derive better-resolution models of the lithosphere from GOCE (see the discussion in Section
697 5).

698 As a further justification for using RRs for GOCE-GGM assessment over CCs, the
699 comparison between the two indicators in Fig 3 shows that CCs are less sensitive to indicate
700 the extent of captured topography signals (seen by the almost constant correlation of $+0.7$
701 between degrees ~ 25 to ~ 150 , while RRs steadily increase) and signal loss (CCs range
702 between $+0.1$ and $+0.5$, while RRs are equally near 0%). Hence, only the correlation
703 between model and topography-implied gravity cannot be recommended as a sole indicator
704 for GGM analysis.

705

706 **4.4 Regional comparisons with RET2011**

707 Figure 6 shows the differences between TIM2 and EGM2008 gravity in the same
708 spectral band of degrees 2 to 200. The agreement is satisfactory over wide parts of the
709 oceans, Europe, North America and Australia (areas where EGM2008 is partially based on
710 dense altimetric and terrestrial gravity data), while large differences are present over parts of
711 Asia, Africa, South America and Antarctica [see also *Hirt et al.*, 2011; *Pail et al.*, 2011;
712 *Rummel et al.*, 2011]. These are regions of rather poor terrestrial gravity availability, and
713 where GOCE is expected to add significantly to gravity field knowledge. It was argued by
714 *Hirt et al.* [2011]: “*Large differences, occurring over [these] regions [...], indicate GOCE*
715 *may improve over EGM2008. However, since there are no ground truth data in these*
716 *regions, it is only possible to make an inference*“.

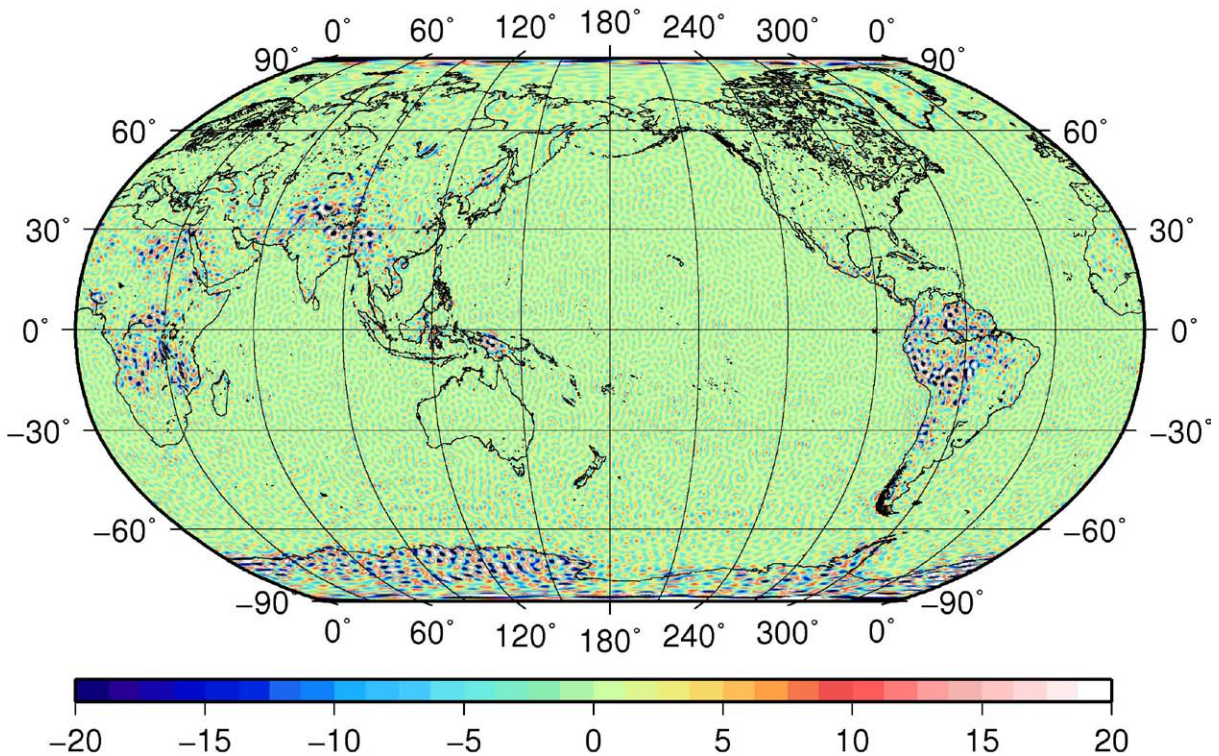
717
718
719

Table 2. Effective spherical harmonic degree for each GGM (cf. Table 1) as inferred by Eq. (20).

Model	World ^a	Himalayas ^b	Andes ^c	Africa ^d	New Guinea ^e	Antarctica ^f
ITG-Grace2010s	168	172	168	168	166	164
GOCE-SPW2	196	196	180	190	180	196
GOCE-SPW1	196	190	180	176	184	164
GOCE-DIR3	220	200	180	200	196	202
GOCE-DIR2	202	198	180	176	188	190
GOCE-DIR1	n/o	n/o	224	n/o	196	222
GOCE-TIM3	222	208	190	186	200	222
GOCE-TIM2	202	200	190	186	196	202
GOCE-TIM1	196	172	180	176	188	164

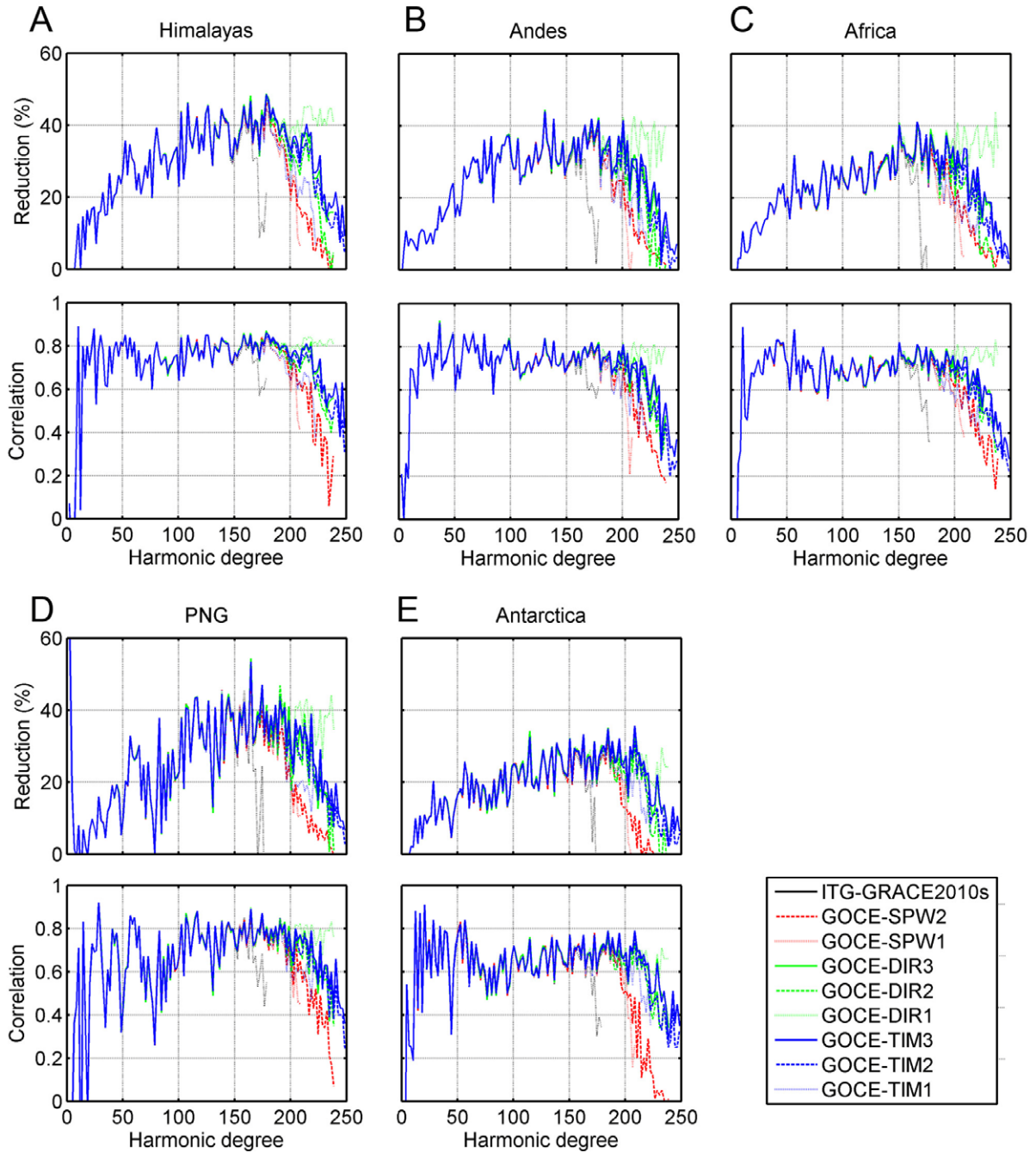
720
721
722
723
724
725
726

a $-83.3^\circ \leq \varphi \leq 83.3^\circ$, $-180^\circ \leq \lambda \leq 180^\circ$ b $20^\circ \leq \varphi \leq 45^\circ$, $65^\circ \leq \lambda \leq 110^\circ$
c $-80^\circ \leq \varphi \leq -60^\circ$, $-40^\circ \leq \lambda \leq 10^\circ$ d $-30^\circ \leq \varphi \leq 30^\circ$, $10^\circ \leq \lambda \leq 40^\circ$
e $-10^\circ \leq \varphi \leq 0^\circ$, $130^\circ \leq \lambda \leq 150^\circ$ f $-83.3^\circ \leq \varphi \leq -70.0^\circ$, $-180^\circ \leq \lambda \leq 180^\circ$
n/o = not observed



727
728
729
730

Fig. 6. Differences between gravity from EGM2008 and GOCE-TIM2, spectral band 2 to 200, Robinson projection, units in mGal.



731

732

733

734

735

736

737

738

739

740

741

742

Fig. 7. Reduction rates and cross-correlation coefficients between RET2011 and GGM gravity as a function of degree n for five regional study areas: A: Himalaya ($20^\circ \leq \varphi \leq 45^\circ$ and $65^\circ \leq \lambda \leq 110^\circ$), B: Andes ($-40^\circ \leq \varphi \leq 10^\circ$ and $-80^\circ \leq \lambda \leq -60^\circ$), C: Africa ($-30^\circ \leq \varphi \leq 30^\circ$ and $10^\circ \leq \lambda \leq 40^\circ$), D: Papua New Guinea (PNG) ($-10^\circ \leq \varphi \leq 0^\circ$ and $130^\circ \leq \lambda \leq 150^\circ$), E: Antarctic ($-83.3^\circ \leq \varphi \leq -70.0^\circ$ and $-180^\circ \leq \lambda \leq 180^\circ$); the legend for all panels is shown in the bottom right.

Over the regions in Fig 7, we benchmark GOCE improvements by means of topography-implied gravity with data extending over the entire areas for the first time. Our evaluation offers some compromise in the interim until terrestrial/airborne gravimetry can be collected to provide real ground-truth, or the proprietary data sets [cf. Pavlis *et al.*, 2008] are declassified. We have chosen five regions of relatively poor ground gravity coverage – the

743 Himalayas, Andes, Africa, Papua New Guinea and Antarctica (North of the -83.3° parallel) –
744 which are marked in Fig. 2. Over each of these regions, RRs (and for the sake of
745 completeness CCs) are shown in Fig. 7. The effective degrees computed from Eq. (20) are
746 reported in Table 2. In comparison with Fig. 5, oscillations of the indicators are stronger,
747 which is due to the limited extent of the test regions. Over all regions, the comparisons
748 between the GOCE GGMs and topography-implied gravity show unanimously that

- 749 • the second (third) generation GOCE gravity values are in close agreement with
750 topography-implied gravity up to degree ~ 200 (~ 220),
- 751 • the second-generation of GOCE models improves upon the first generation in band
752 ~ 185 to ~ 200 , and
- 753 • GOCE delivers improved gravity field knowledge in band ~ 165 to ~ 200 compared
754 with GRACE.

755 Over all regions, the GOCE-TIM2 (TIM3) solution appears to offer the best performance,
756 marginally better than GOCE-DIR2 (DIR3) and notably better than GOCE-SPW2 at short
757 scales. The agreement between topography and DIR1 reflects that it incorporates altimetry
758 and terrestrial gravity data (and, most likely, topography information) in the high spectral
759 degrees. Over the rugged Himalaya and Papua New Guinea areas, RRs are close to $\sim 50\%$,
760 indicating that the topography is a dominant source of the gravity field over these areas. Over
761 all of our test regions, GOCE-TIM3 captures RET-implied signals even in harmonic band
762 240 to 250, which follows from the slightly positive RRs, or, in other words, from the simple
763 observation that subtracting GOCE-TIM3 from RET-implied gravity reduces the RMS-signal
764 strength of the latter [cf. Eq. (19)]. This behavior demonstrates that 12 months satellite
765 gravimetry observations capture information on Earth's gravity field in attenuated form down
766 to ~ 80 km spatial scales.

767

768 **5. Discussion and Conclusions**

769 Degree-wise comparisons between GOCE and gravity implied by Earth's topography
770 show that the second- and third-generation GOCE GGMs add significantly to Earth gravity
771 field knowledge over the Himalayas, Andes, Africa, Papua New Guinea and Antarctica,
772 regions with poor or classified ground gravity coverage and where conventional GGM
773 evaluation can be difficult.

774 Comparisons were made among eight official ESA GOCE models, based on ~ 2 , ~ 8
775 and ~ 12 months of space gravimetry observations. These first, second and third-generation
776 GOCE models gradually improve over ITG-GRACE2010s from the pre-GOCE-era, with the
777 third-generation GOCE GGMs enhancing our gravity field knowledge from harmonic degree
778 ~ 165 to ~ 200 - 220 , or from spatial scales of ~ 120 km down to ~ 90 - 100 km, both globally and
779 regionally.

780 Our comparisons provide some feedback on ESA's three current GOCE gravity
781 recovery philosophies: direct (DIR), time-wise (TIM) and space-wise (SPW), and on the
782 effective model resolution, indicating the highest degree where they seem to possess almost
783 full spectral power. Based on second-generation comparisons, the TIM and DIR approaches
784 offer a better agreement with topography-implied signals than the SPW approach. Both for
785 the second- and third generation models, the TIM and DIR approaches showed similarly

786 close agreement with topography-implied gravity, and the third-generation GOCE models
787 were found to capture most of topography-generated gravity field signal to spherical
788 harmonic degrees of ~200-220.

789 Despite being theoretically a poorer description of the Earth's uppermost mass
790 distribution, the uncompensated topography turned out to be a data source that seems suitable
791 for providing feedback on GOCE gravity field models. The spatial resolution of current
792 lithosphere models based on observations (from seismic refraction data or elastic thicknesses
793 estimates) is not fine enough to provide a feedback on the GOCE gravity models everywhere
794 on Earth.

795 Therefore, in the absence of better strategies, isostasy was tested based on the
796 classical though simplistic models of Airy/Heiskanen and Pratt/Hayford, and a hybrid
797 combination of them, because these hypotheses [formally] offer a spatial resolution
798 commensurate with GOCE. However, failing to confer improvements over the agreement
799 seen among GOCE and the uncompensated topography, the isostasy models tested here –
800 specifically the A/H hypothesis – are of limited benefit to precisely describe isostasy globally
801 at the spatial scales resolved by GOCE.

802 In the absence of an efficient high-resolution description of isostasy, the new GOCE
803 gravity field models may become an important new data source that implicitly contain
804 information on yet unknown mass-density features [cf. *Benedek and Papp, 2009; Braitenberg*
805 *et al., 2010*]. In modeling the density structure of the lithosphere, the GOCE models may
806 serve as important boundary condition [cf. *Marotta, 2003*]. The use of GOCE gravity
807 observations specifically for improved recovery of crustal thicknesses (Moho recovery) has
808 been proposed or is under investigation [e.g., *Braitenberg et al., 2010; Tedla et al., 2010;*
809 *Bagherbandi, 2011; Köther et al., 2011; Reguzzoni and Sampietro 2012*].

810 The third-generation GOCE models resolve the Earth's gravity field at spatial scales
811 not recovered before by other space gravimetry missions. Showing the closest agreement
812 with topography-implied signals, the TIM3 and DIR3 models are recommended as “currently
813 the best” medium-wavelength space-collected data sources to describe the gravity field over
814 some regions. Further improvements should be anticipated from future GOCE model
815 generations that are based on data volumes larger than ~12 months.

816 At spatial scales as short as ~80-90 km (harmonic degrees of 220 to 250), our
817 comparisons revealed topography-generated gravity signals captured [albeit in attenuated
818 form] by the third-generation GOCE gravity field models. This demonstration of GOCE's
819 ability for short-scale signal recovery down to ~80-90 km scales suggests that short-
820 wavelength gravity signals originating from e.g., the crust-mantle boundary and buried
821 anomalous mass loads are captured as well, making the new GOCE data sets a promising
822 source to improve our knowledge on the Earth's lithosphere structure.

823

824 **Acknowledgements**

825 We would like to thank the Australian Research Council (ARC) for funding through
826 discovery project grants DP0663020 and DP120102441. CH is the recipient of an ARC
827 Discovery Outstanding Researcher Award (DORA). MK is the recipient of a Curtin Research
828 Fellowship. We also thank the editor and reviewers for their comments on the manuscript,

829 directing us to include isostatic compensation models in this study. We thank ESA for
830 making the new GOCE gravity fields freely available. Thanks go also to the EGM2008
831 development team for the topography data. Some figures were produced using the Generic
832 Mapping Tools (GMT; *Wessel and Smith* [1998]).

833

834 **References**

- 835 Abdalati, W., H.J. Zwally, R. Bindenschadler, B. Csatho, S.L. Farrell, H.A. Fricker, D.
836 Harding, R. Kwok, M. Lefsky, T. Markus, A. Marshak, T. Neumann, S. Palm, B.
837 Schutz, B. Smith, J. Spinhirne, and C. Webb (2010), The ICESat-2 Laser Altimetry
838 Mission, *Proceedings of the IEEE*, Vol. 98, No. 5, pp. 735-751.
- 839 Amante, C., and B.W. Eakins (2009), ETOPO1 1 arc-minute global relief model: Procedures,
840 Data Sources and Analysis, NOAA Technical Memorandum NESDIS NGDC-24, 19 p.
- 841 Bagherbandi, M. (2011), An isostatic Earth crustal model and its applications, Doctoral
842 Dissertation, *Division of Geodesy and Geoinformatics*, Royal Institute of Technology
843 (KTH) Sweden. URL: kth.diva-portal.org/smash/get/diva2:407999/FULLTEXT01
- 844 Bamber, J.L., R.L. Layberry, and S.P. Gogenini (2001), A new ice thickness and bed data set
845 for the Greenland ice sheet 1: Measurements, data reduction, and errors, *J. Geophys.*
846 *Res.*, 106(D24), 33773-33780.
- 847 Bassin, C., G. Laske, T.G. Masters (2000), The current limits of resolution for surface wave
848 tomography in North America, *EOS Trans AGU*, 81:F897.
- 849 Benedek, J., and G. Papp (2009), Geophysical inversion of on board satellite gradiometer
850 data. a feasibility study in the Alpaca region, Central Europe. *Acta Geod. Geoph.*
851 *Hung.*, 44(2), 179-190, DOI: 10.1556/AGeod.44.2009.2.4.
- 852 Bock, H., A. Jaeggi, U. Meyer, P. Visser, J. van den Ijssel, T. van Helleputte, M. Heinze, and
853 U. Hugentobler (2011), GPS-derived orbits for the GOCE satellite, *J. Geod.*, 85(11),
854 807–818, DOI: 10.1007/s00190-011-0484-9.
- 855 Braitenberg, C., P. Mariani, M. Reguzzoni, and N. Ussami (2010), GOCE observations for
856 detecting unknown tectonic features, In: Proc. ‘ESA Living Planet Symposium’,
857 Bergen, Norway 28 June – 2 July 2010 (ESA SP-686).
- 858 Bruinsma SL, Lemoine JM, Biancale R, Vales N (2009), CNES/GRGS 10-day gravity field
859 models (release 2) and their evaluation, *Adv. Space Res.*, 45(4), 587-601,
860 doi:10.1016/j.asr.2009.10.012.
- 861 Bruinsma, S.L., J.C. Marty, G. Balmino, R. Biancale, C. Förste, O. Abrikosov, and H.
862 Neumayer (2010), GOCE Gravity Field Recovery by Means of the Direct Numerical
863 Method, *Presented at the ESA Living Planet Symposium 2010*, Bergen, June 27 – July 2
864 Bergen, Norway.
- 865 Colombo, O.L. (1981), Numerical methods for harmonic analysis on the sphere, Report no.
866 310, *Department of Geodetic Science*, Ohio State University, Columbus.
- 867 Drinkwater, M.R., R. Floberghagen, R. Haagmans, D. Muzi, and A. Popescu (2003), GOCE:
868 ESA’s first Earth Explorer Core mission, In (eds. Beutler, G.B., M.R. Drinkwater, R.
869 Rummel, and R. von Steiger), *Earth Gravity Field from Space - from Sensors to Earth*
870 *Sciences*. In the Space Sciences Series of ISSI, Vol. 18, 419-432, Kluwer Academic
871 Publishers, Dordrecht, Netherlands ISBN: 1-4020-1408-2.

872 EGM Team (2008), Earth Gravitational Model 2008 – readme files. URL: <http://earth->
873 [info.nga.mil/GandG/wgs84/gravitymod/egm2008](http://earth-info.nga.mil/GandG/wgs84/gravitymod/egm2008).

874 Farr, T.G., P.A. Rosen, E. Caro, R. Crippen, R. Duren, S. Hensley, M. Kobrick, M. Paller, E.
875 Rodriguez, L. Roth, D. Seal, S. Shaffer, J. Shimada, J. Umland, M. Werner, M. Oskin,
876 D. Burbank, and D. Alsdorf (2007), The Shuttle Radar Topography Mission, *Rev.*
877 *Geophys.*, 45, RG2004, doi:10.1029/2005RG000183.

878 Förste, C., S. Bruinsma, R. Shako, J.C. Marty, F. Flechtner, O. Abrikosov, C. Dahle, J.M.
879 Lemoine, H. Neumayer, R. Biancale, F. Barthelmes, R. König, and G. Balmino (2011),
880 EIGEN-6 - A new combined global gravity field model including GOCE data from the
881 collaboration of GFZ-Potsdam and GRGS-Toulouse, *Geophysical Research Abstracts*
882 Vol. 13, EGU2011-3242-2, 2011 EGU General Assembly, Vienna.

883 Forsberg R., and C.C. Tscherning (1981), The use of height data in gravity field
884 approximation by collocation, *J. Geophys. Res.*, 86(B9), 7843-7854.

885 Goiginger H., E. Hoeck, D. Rieser, T. Mayer-Guerr, A. Maier, S. Krauss, R. Pail, T. Fecher,
886 T. Gruber, J.M. Brockmann, I. Krasbutter, W.-D. Schuh, A. Jaeggi, L. Prange, W.
887 Hausleitner, O. Baur, and J. Kusche (2011), The combined satellite-only global gravity
888 field model GOCO02S, *Geophysical Research Abstracts*. Vol. 13, EGU2011-10571,
889 2011 EGU General Assembly, Vienna.

890 Götzl, F., and R. Rummel (2009), A Geodetic View on Isostatic Models. *Pure Appl. Geoph.*,
891 166(8-9), 1247-1260, DOI: 10.1007/s00024-004-0489-x.

892 Gruber, T., P.N.A.M Visser, C. Ackermann, and M. Hosse (2011), Validation of GOCE
893 gravity field models by means of orbit residuals and geoid comparisons, *J Geod.*,
894 85(11), 845-860, DOI 10.1007/s00190-011-0486-7.

895 Heiskanen W.A., and H. Moritz (1967), *Physical Geodesy*, W.H. Freeman and Company, San
896 Francisco.

897 Hirt, C., W.E. Featherstone and U. Marti (2010a) Combining EGM2008 and
898 SRTM/DTM2006.0 residual terrain model data to improve quasigeoid computations in
899 mountainous areas devoid of gravity data, *J. Geod.*, 84(9): 557-567, DOI:
900 10.1007/s00190-010-0395-1.

901 Hirt, C., U. Marti, B. Bürki, and W.E. Featherstone (2010b), Assessment of EGM2008 in
902 Europe using accurate astrogeodetic vertical deflections and omission error estimates
903 from SRTM/DTM2006.0 residual terrain model data, *J. Geophys. Res. Solid Earth*,
904 115, B10404, DOI:10.1029/2009JB007057.

905 Hirt, C., T. Gruber, W.E. Featherstone (2011), Evaluation of the first GOCE static gravity
906 field models using terrestrial gravity, vertical deflections and EGM2008 quasigeoid
907 heights. *J. Geod.*, 85(10): 723-740, DOI: 10.1007/s00190-011-0482-y.

908 Holmes, S.A., and N.K. Pavlis (2008), Spherical harmonic synthesis software
909 `harmonic_synth`.
910 URL: http://earth-info.nga.mil/GandG/wgs84/gravitymod/new_egm/new_egm.html

911 Janák, J., F. Wild-Pfeiffer and B. Heck (2012), Smoothing the Gradiometric Observations
912 Using Different Topographic–Isostatic Models: A Regional Case Study, VII Hotine-
913 Marussi Symposium on Mathematical Geodesy, *IAG Symposia Series* 137(5), 245-250,
914 DOI: 10.1007/978-3-642-22078-4_37.

915 Kaula, W.M. (1966), *Theory of Satellite Geodesy*. Blaisdel, Waltham.

916 Köther, N., H.-J. Götze, B.D. Gutknecht, T. Jahr, G. Jentzsch, O.H. Lücke, R. Mahatsente, R.
917 Sharm, and S. Zeumann (2011), The seismically active Andean and Central American
918 margins: Can satellite gravity map lithospheric structures? *Journal of Geodynamics*,
919 (online first), DOI:10.1016/j.jog.2011.11.004.

920 Kuhn, M., and W.E. Featherstone (2003), On the optimal spatial resolution of crustal mass
921 distributions for Forward Gravity Field Modelling, In: *Proceed 3rd Meeting of the*
922 *Intern. Gravity and Geoid Commission*, (ed. I Tziavos), Ziti Editions, pp 195-200.

923 Lythe, M.B., D.G. Vaughan, and BEDMAP consortium (2000), BEDMAP – bed topography
924 of the Antarctic, 1:10,000,000 scale map, BAS (Misc) 9, Cambridge, British Antarctic
925 Survey.

926 Marotta, A. (2003), Benefits from GOCE within solid Earth geophysics, *Space Science*
927 *Reviews* 108, 95-104.

928 Mayer-Gürr, T., E. Kurtenbach, and A. Eicker (2010), ITG-Grace2010 Gravity Field Model.
929 URL: <http://www.igg.uni-bonn.de/apmg/index.php?id=itg-grace2010>, 2010.

930 Makhloof, A.A. (2007), *The Use of Topographic-Isostatic Mass Information in Geodetic*
931 *Applications*, Dissertation. Institut für Geodäsie und Geoinformation der Universität
932 Bonn, D 98.

933 Makhloof, A.A., and K.-H. Ilk (2008), Effects of topographic–isostatic masses on
934 gravitational functionals at the Earth’s surface and at airborne and satellite altitudes. *J*
935 *Geod*, 82(2), 93–111, DOI 10.1007/s00190-007-0159-8.

936 Mladek, F. (2006), *Hydrostatische Isostasie*, Schriftenreihe IAPG/FESG No. 24, Institut für
937 *Astronomische und Physikalische Geodäsie*, TU München.
938 URL: http://www.iapg.bv.tum.de/mediadb/9853/9854/iapg_fesg_rpt_24.pdf

939 Migliaccio, F., M. Reguzzoni, F. Sanso, C.C. Tscherning, and M. Veicherts (2010), GOCE
940 data analysis: the space-wise approach and the first space-wise gravity field model.
941 Presented at the ESA Living Planet Symposium 2010, Bergen, June 27 - July 2,
942 Bergen, Norway.

943 Novák, P., and E. W. Grafarend (2006), The effect of topographical and atmospheric masses
944 on spaceborne gravimetric and gradiometric data. *Stud. Geophys. Geod.* 50(4), 549-
945 582, DOI: 10.1007/s11200-006-0035-7

946 Pail, R., Goiginger, H., W.-D. Schuh, E. Höck, J.M. Brockmann, T. Fecher, T. Gruber, T.
947 Mayer-Gürr, J. Kusche, A. Jäggi, and D Rieser (2010), Combined satellite gravity field
948 model GOCO01S derived from GOCE and GRACE, *Geophys. Res. Lett.* 37, L20314,
949 DOI: 10.1029/2010GL044906.

950 Pail, R., S. Bruinsma, F. Migliaccio, C. Förste, H. Goiginger, W.-D. Schuh, E. Höck, M.
951 Reguzzoni, J.M. Brockmann, O. Abrikosov, M. Veicherts, T. Fecher, R. Mayrhofer, I.
952 Krasbutter, F. Sansò, and C.C. Tscherning (2011), First GOCE gravity field models
953 derived by three different approaches, *J Geod.*, 85(11), 819-843, DOI:
954 10.1007/s00190-011-0467-x.

955 Pavlis, N.K., J.K. Factor, and S.A. Holmes (2007), Terrain-related gravimetric quantities
956 computed for the next EGM, *Proceedings of the 1st International Symposium of the*
957 *International Gravity Field Service (IGFS)*, Istanbul, pp 318-323.

- 958 Pavlis N.K., S.A. Holmes, S.C. Kenyon, and J.K. Factor (2008), An Earth Gravitational
 959 Model to Degree 2160: EGM2008, Presented at the 2008 General Assembly of the
 960 European Geoscience Union, Vienna, Austria, April 13-18, 2008.
- 961 Rapp, R.H. (1982), Degree variances of the Earth's potential, topography and its isostatic
 962 compensation. *Bulletin Geodesique* 56(2), 84-94.
- 963 Reguzzoni, M. and D. Sampietro (2012), Moho Estimation Using GOCE Data: A Numerical
 964 Simulation, In: *Proceed. Geodesy for Planet Earth, IAG Symposia Series* 136(2), 205-
 965 214, DOI: 10.1007/978-3-642-20338-1_25
- 966 Rummel, R., R.H. Rapp, H. Sünkel, and C.C. Tscherning (1988), Comparisons of global
 967 topographic/isostatic models to the Earth's observed gravity field, Report No 388, *Dep.*
 968 *Geodetic Sci. Surv.*, Ohio State University, Columbus, Ohio.
- 969 Rummel, R., W. Yi, and C. Stummer (2011), GOCE gravitational gradiometry. *J. Geod.*,
 970 85(11), 777-790, DOI: 10.1007/s00190-011-0500-0.
- 971 Saleh, J. and N.K. Pavlis (2003), The development and evaluation of the global digital terrain
 972 model DTM2002, In: *Proceed 3rd Meeting of the Intern. Gravity and Geoid*
 973 *Commission*, (ed. I Tziavos), Editions Ziti, pp. 207-212.
- 974 Smith, W.H.F. and D.T. Sandwell (1997), Global sea floor topography from satellite
 975 altimetry and ship depth soundings, *Science*, 277, 1956-1962.
- 976 Tapley, B. D., S. Bettadpur, M. Watkins, and C. Reigber (2004), The gravity recovery and
 977 climate experiment: Mission overview and early results, *Geophys. Res. Lett.*, 31,
 978 L09607, doi:10.1029/2004GL019920.
- 979 Tedla, G.E., M. van der Meijde, and A. Nyblade (2010), Crustal modeling in Africa; towards
 980 high resolution models using GOCE satellite gravity data, *AGU Fall Meeting 2010*,
 981 abstract #T31C-2188
- 982 Torge, W. (2001), *Geodesy*, 3rd Edition, *de Gruyter*, Berlin, New York.
- 983 Watts, A. B. (2001), *Isostasy and Flexure of the Lithosphere*, *Cambridge University Press*.
- 984 Watts, A. B. (2011), Isostasy, In: *Encyclopedia of Solid Earth Geophysics* (Ed. Gupta, H. K.),
 985 1, 647-662, Elsevier.
- 986 Wessel, P., and W.H.F. Smith (1998), New, improved version of the Generic Mapping Tools
 987 released. *EOS Trans. AGU* 79, 579.
- 988 Wieczorek, M.A. (2007), The gravity and topography of the terrestrial planets. In: Spohn, T.,
 989 Schubert, G. (Eds.), *Treatise on Geophysics*, vol. 10. Elsevier-Pergamon, Oxford, 165-
 990 206.
- 991 Wild, F., and B. Heck, (2005), A comparison of different isostatic models applied to satellite
 992 gravity gradiometry In: Jekeli, C., Bastos, L., Fernandes (Eds.) *Gravity, Geoid and*
 993 *Space Missions*, Porto, Portugal,, IAG Symposia Series 129, 230-235.